Progress in Biophysics and Molecular Biology 104 (2011) 22–48

Contents lists available at ScienceDirect

Progress in Biophysics and Molecular Biology

journal homepage: www.elsevier.com/locate/pbiomolbio

Review

Models of cardiac tissue electrophysiology: Progress, challenges and open questions

R.H. Clayton [a,*], O. Bernus [b], E.M. Cherry [c], H. Dierckx [d], F.H. Fenton [c], L. Mirabella [e,f], A.V. Panfilov [g], F.B. Sachse [h], G. Seemann [i], H. Zhang [j]

[a] Department of Computer Science, University of Sheffield, Regent Court, 211 Portobello Street, Sheffield S1 4DP, UK
[b] Institute of Membrane and Systems Biology, Multidisciplinary Cardiovascular Research Centre, University of Leeds, UK
[c] Department of Biomedical Sciences, Cornell University, Ithaca, NY, USA
[d] Department of Physics and Astronomy, University of Ghent, Belgium
[e] Department of Mathematics and Computer Science, Emory University, USA
[f] Dipartimento di Matematica, Politecnico di Milano, Italy
[g] Department of Theoretical Biology, Utrecht University, The Netherlands
[h] Bioengineering Department and Nora Eccles Harrison Cardiovascular Research and Training Institute, University of Utah, USA
[i] Institute of Biomedical Engineering, Karlsruhe Institute of Technology, Germany
[j] Department of Physics, University of Manchester, UK

ARTICLE INFO

Article history:
Available online 27 May 2010

Keywords:
Computer model
Cardiac tissue
Electrophysiology
Heart
Review

ABSTRACT

Models of cardiac tissue electrophysiology are an important component of the Cardiac Physiome Project, which is an international effort to build biophysically based multi-scale mathematical models of the heart. Models of tissue electrophysiology can provide a bridge between electrophysiological cell models at smaller scales, and tissue mechanics, metabolism and blood flow at larger scales. This paper is a critical review of cardiac tissue electrophysiology models, focussing on the micro-structure of cardiac tissue, generic behaviours of action potential propagation, different models of cardiac tissue electrophysiology, the choice of parameter values and tissue geometry, emergent properties in tissue models, numerical techniques and computational issues. We propose a tentative list of information that could be included in published descriptions of tissue electrophysiology models, and used to support interpretation and evaluation of simulation results. We conclude with a discussion of challenges and open questions.

Contents

* Corresponding author. Tel.: +44 114 222 1845; fax: +44 114 222 1810.
E-mail addresses: r.h.clayton@sheffield.ac.uk (R.H. Clayton), o.bernus@leeds.ac.uk (O. Bernus), emc58@cornell.edu (E.M. Cherry), hans.dierckx@ugent.be (H. Dierckx), fhf3@cornell.edu (F.H. Fenton), lucia@mathcs.emory.edu (L. Mirabella), a.panfilov@uu.nl (A.V. Panfilov), fs@cvrti.utah.edu (F.B. Sachse), Gunnar.Seemann@kit.edu (G. Seemann), h.zhang-3@manchester.ac.uk (H. Zhang).

0079-6107/$ – see front matter © 2010 Elsevier Ltd. All rights reserved.
doi:10.1016/j.pbiomolbio.2010.05.008

1. Introduction

Mechanical contraction of cardiac tissue is triggered by electrical depolarisation of the cell membrane, and co-ordinated by the spread of depolarisation through cardiac tissue from the sino-atrial node to other regions of the heart. The sequence of depolarisation and subsequent repolarisation can be measured with electrodes (Durrer et al., 1970) and optical imaging using voltage-sensitive fluorescent dyes (Efimov et al., 2004). These experimental techniques have been especially valuable for documenting the abnormal activation patterns that underlie cardiac arrhythmias (Gray et al., 1998).

Cardiac tissue contains excitable myocytes. Local depolarisation of the cardiac myocyte membrane above a threshold voltage, for example in response to current injection from a stimulating electrode or current provided by neighbouring myocytes, triggers the opening of voltage-gated Na^+ channels and a rapid membrane depolarisation, which generates an action potential. The action potential upstroke produces local gradients in membrane voltage that cause current flow within the tissue. This current flow acts in turn to open voltage-gated Na^+ channels in neighbouring electrically connected cells, resulting in propagation of the action potential through the tissue (Jongsma and Wilders, 2000; Kleber and Rudy, 2004; Plonsey and Barr, 2000; Rook et al., 1992). The speed and pattern of propagation depends on local tissue micro-structure, although at larger spatial scales cardiac tissue behaves as a functional syncytium.

Over the last 50 years, experimental cardiac electrophysiology has been increasingly complemented by computational models of action potential propagation that embed models of membrane excitability within a framework that describes cardiac tissue (Clayton and Panfilov, 2008; Henriquez and Papazogou, 1996; Kleber and Rudy, 2004). These models can provide a quantitative description of action potential propagation, and have explanatory power because they can be used to test and generate hypotheses that are difficult to address experimentally. Examples where models have provided new insights include studying the mechanisms of re-entry and defibrillation in 3D tissue (Rodriguez et al., 2005; Ten Tusscher et al., 2009), and the role of tissue micro-structure and heterogeneity in the atrioventricular node (Li et al., 2008). While it appears conceptually straightforward to build models of cardiac tissue electrophysiology, these models typically

embed several important assumptions. The model assumptions can have important implications for the interpretation of simulation studies. For instance, most models of cardiac electrophysiology assume that cardiac tissue can be treated as a static continuum, where parameter values such as tissue conductivity are either uniformly distributed or vary smoothly in space. Furthermore, most models assume that cardiac tissue is comprised of myocytes and extracellular space only. These models neglect other types of cells and compartments. Similarly, assumptions of modelling parameter values can have important consequences for the accuracy and validity of models, yet many parameter values are difficult to obtain and to verify (Winfree, 1998).

Models of tissue electrophysiology are an important component of the Cardiac Physiome Project, which is an international effort to build biophysically based multi-scale mathematical models of the heart. Models of tissue electrophysiology can provide a bridge between electrophysiological cell models, tissue mechanics, and blood flow (see other papers in this issue). This paper is a critical review of computational models of action potential propagation in tissue, with a focus on six main areas. First, we cover the structure and micro-structure of cardiac tissue, and how this structure determines the passive electrical properties of bulk tissue. Second, we review the generic behaviours of action potential propagation in 1-D, 2-D, and 3-D tissue. Third, we discuss different approaches to modelling cardiac tissue, the choice of parameter values, and tissue geometry. Fourth, we examine the implications of embedding excitable cells into tissue, both for models and for real tissue. Fifth, we review commonly used numerical approaches to solving the models described in section three. Sixth, we discuss ways to reduce computation times. We finish with a discussion of challenges and open questions in electrophysiological tissue modelling.

2. Cardiac tissue micro-structure and electrical properties

At the microscopic level, cardiac muscle is a composite tissue. It consists of various cell types, mainly myocytes and fibroblasts, supported by an extracellular matrix (ECM) and permeated by fluids. In this section we provide a brief overview of the major components of cardiac muscle at the microscopic level, how the components are organised spatially in the heart, and how the tissue micro- and macrostructure influence the passive electrical properties of cardiac tissue.

2.1. Cellular components of myocardium

2.1.1. Myocytes

Cardiac myocytes are the major constituent of heart muscle, and their primary function is to produce mechanical tension. Contraction is triggered by electrical depolarisation, which is initiated and mediated by specialised myocytes including sino-atrial and atrioventricular node cells and Purkinje cells (Boyett et al., 2009; Hucker et al., 2009). In mammalian atrial and ventricular tissue, myocytes can be coarsely approximated by a cylinder with dimensions ranging from 50 to 150 μm in length and 10–20 μm in diameter (Gerdes et al., 1986; Satoh et al., 1996; Spach et al., 2004; Streeter et al., 1969). The shape and volume of myocytes even in a small region of tissue can be variable and complex, and these properties are also influenced by species, developmental stage, and disease processes (Bers, 2008; Campbell et al., 1987).

Myocytes are enclosed by a lipid membrane, the sarcolemma, which separates the cell exterior from its interior. Cardiac myocytes contain one or more nuclei, usually in the cell centre. On average a mature young (17–30 years) healthy human heart contains approximately 8.2 billion myocyte nuclei in the ventricles (Olivetti et al., 1991), corresponding to about 6.5 billion cells, assuming that 25 percent of myocytes have two nuclei and 75 percent one nucleus (Olivetti et al., 1996). An average annual loss of approximately 52 million ventricular myocyte nuclei per year ensues subsequently, with a corresponding increase in ventricular myocyte volume of 110–120 μm^3 per year (Olivetti et al., 1991) acting to preserve thickness.

Cardiac myocytes also contain mitochondria, myofibrils, the sarcoplasmic reticulum, the sarcomeres and the cytoskeleton, which provides anchoring for the different organelles. The intracellular space is filled up with the sarcoplasm, an aqueous solution containing lipids, various ion species, carbon hydrates and proteins. The sarcolemma represents a semi-permeable barrier, and contains the ion channel, pump, and exchanger proteins that carry the inward and outward currents that underlie the action potential, as well as proteins involved in cell adhesion and signalling. Expression of these membrane proteins is strongly dependent on developmental stage, tissue type, and location, and is further influenced by disease. Transverse tubules (t-tubules) are deep invaginations of the sarcolemma, and act to communicate electrical and Ca^{2+} signals to the cell interior (Brette and Orchard, 2003; Fawcett and McNutt, 1969). The t-tubules have a complex geometry (Fig. 1), with a high density of L-type Ca^{2+} channels located closely to Ca^{2+} release sites in the sarcoplasmic reticulum. A further specialisation of the cell membrane is found at its ends, i.e. the intercalated disks, where cells are mechanically coupled. Intercalated disks also include gap junction channels, which provide for intercellular electrical coupling (see below) (Gumbiner, 1996; Lodish et al., 2003).

2.1.2. Fibroblasts

Although myocytes account for the largest volume fraction of normal myocardium, they can be outnumbered by the much smaller fibroblasts (Adler et al., 1981; Camelliti et al., 2005). The density of fibroblasts in cardiac muscle is dependent on species, age and disease (Banerjee et al., 2007, 2006). Cardiac fibroblasts play a major role in the maintenance of the ECM, which provides a framework for cardiac tissue and is the major determinant of passive mechanical properties. Fibroblasts can develop into myofibroblasts. Both cell types serve as mediators of inflammatory responses and are involved in the development of fibrosis in the injured heart.

2.1.3. Other cell types

Endothelial cells cover the internal surface of blood vessels in cardiac tissue (Davies, 2009), and vascular smooth muscle cells are found in vessel walls. Various types of neural cell are also associated with innervation of the myocardium (Chen and Chen, 2009).

2.2. Spatial organisation

2.2.1. Gap junctions, fibres and sheets

Myocytes are coupled to other myocytes by gap junction channels, which enable both intercellular signalling and propagation of the action potential as described in Section 3 (Delmar and Sorgen, 2009; Lampe and Fishman, 2009; van Kempen et al., 1991). Gap junctions have a cylindrical or barrel shape with a diameter of about 2 nm and length of approximately 2–12 nm. Gap junction channels consist of two hemi-channels, connexons, located in the membrane of the two coupled cells. Each connexon is formed by six membrane proteins, connexins, which have been named according to their atomic weight ranging from 25 to 50 kD. In mammalian ventricular myocardium connexin43 is the most prevalent. Other connexins have been found in the atria and conduction system (connexin37, connexin40 and connexin45).

Gap junctions can be found at various locations throughout the sarcolemma, but most are located at intercalated disks. Longitudinally coupled gap junctions are found at the longitudinal ends of

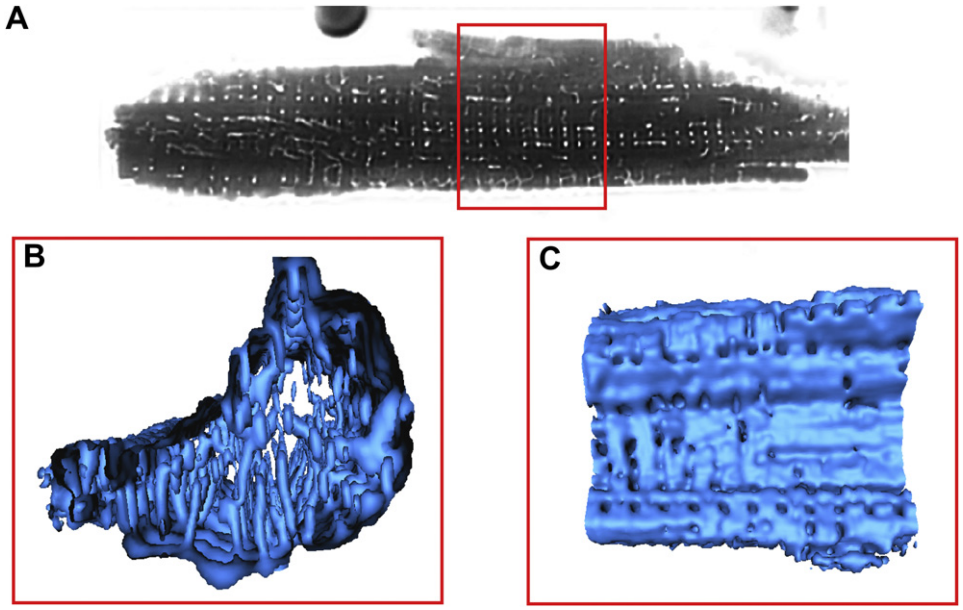

Fig. 1. Confocal microscopy of isolated living ventricular myocyte from rabbit (modified from (Savio-Galimberti et al., 2008)). (A) A transversal section through the myocyte is shown with the cell interior in dark and exterior in bright color. (B, C) A segment of cell is visualised in three dimensions. The cell membrane includes deep invaginations, the transverse tubular system, into the cell interior.

cells, whereas transverse gap junctions are located in lateral membranes. The distribution of gap junction orientations in the sarcolemma depends on tissue type. In ventricular myocardium, longitudinal gap junctions are most abundant, resulting in macroscopic anisotropic electrical coupling (Hoyt et al., 1989).

The main features of tissue micro-structure are preferential local alignment of myocytes along their principal axis (Fig. 2) and their end-to-end coupling. By analogy to skeletal muscle, a local fibre orientation can be defined along the principal axis of myocytes. In the ventricles, fibre orientation has been known to smoothly rotate between endocardium and epicardium ever since original work by Streeter (Streeter et al., 1969). This finding obtained by visual inspection of tissue has been confirmed using various techniques, such as histology (Streeter et al., 1969), optical techniques (Hucker et al., 2008; Sands et al., 2005; Smith et al., 2008), and diffusion tensor MRI (Gilbert et al., 2007) (Fig. 3). Peskin also used mechanical principles to derive the fibre architecture of the ventricles with a prediction of about 180° of rotation between endocardium and epicardium (Peskin, 1989). Comparative anatomical studies have shown that these general features of fibre organisation in the ventricular wall are conserved across species. Some of these studies however have highlighted specific regions of the myocardium where fibre organisation is much more variable (Dierckx et al., 2009; Nielsen et al., 1991; Scollan et al., 2000), suggesting abrupt changes in orientation and meshing of fibres (Lunkenheimer et al., 2006).

In addition to the fibrous structure described above, ventricular myocytes are organised into laminar structures, also called sheets, which were first described in detail by Feneis and Hort (Hort, 1957a, 1957b, 1960). These sheets are typically 4–6 myocytes thick and are separated by cleavage planes and layers of connective tissue. Detailed microscopic imaging studies of cardiac tissue has demonstrated a laminar structure in ventricular tissue (Sands et al., 2005); however, it is important to note that the laminar structure involves branching and discontinuous sheets that accommodate the fibre structure, and may be more prominent in some parts of the ventricles than others (Gerneke et al., 2007; LeGrice et al., 1995; Pope et al., 2008; Sands et al., 2005). The ventricular wall also accommodates a vascular network, and detailed examination shows the presence of many blood vessels and other voids within the tissue (Burton et al., 2006).

2.2.2. *Regional differences in tissue properties*

The shape and arrangements of myocytes depends on tissue type and so varies with location in the heart, with important differences between atrial and ventricular tissue for example

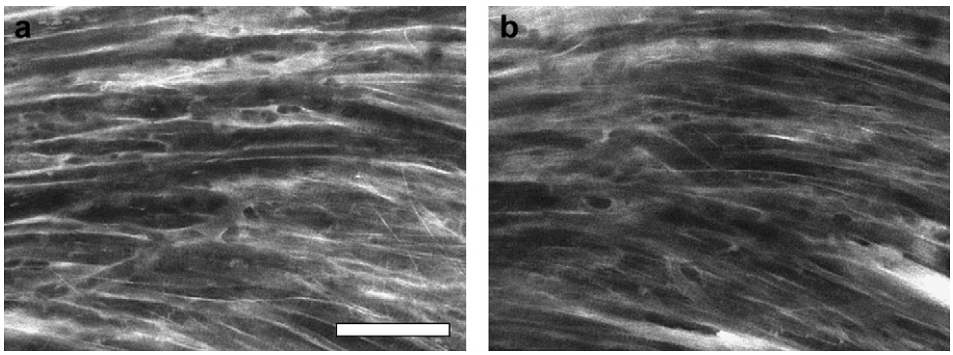

Fig. 2. Confocal microscopic images from a three-dimensional stack of living atrial tissue of rabbit (modified from (Lasher et al., 2009)). The images are acquired at a depth of (a) 20 μm and (b) 30 μm into the sub-epicardial myocardium. Scale: 50 μm.

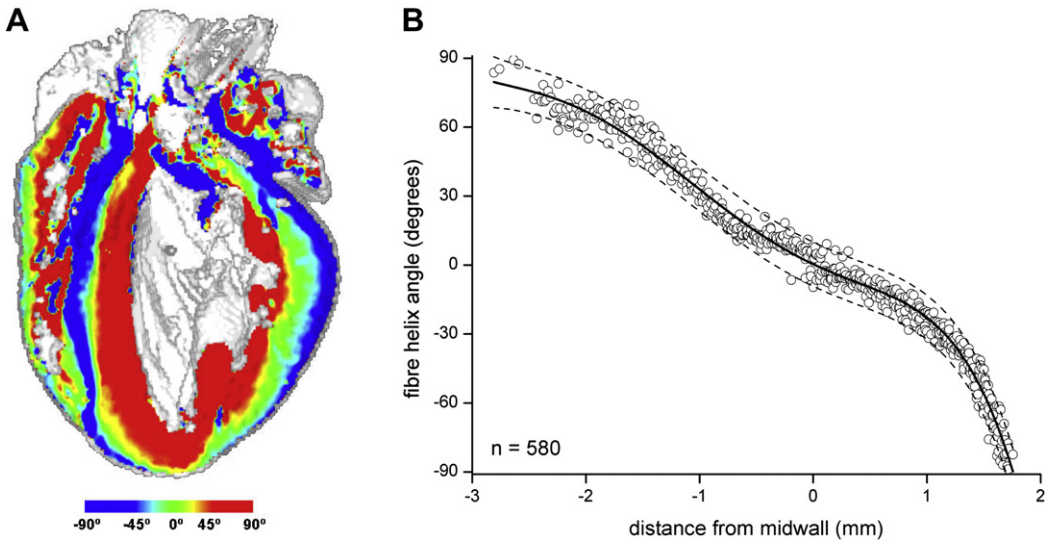

Fig. 3. Reconstruction of fibre orientation in the rabbit heart using DT-MRI. (A) Long-axis cross section through the heart showing fibre helix angle. (B) Transmural fibre helix angles extracted from a sector of the left ventricular mid free wall and fitted with a 5th order polynomial. The dashed lines represent the 95% confidence interval. Modified from (Gilbert et al., 2009).

(Anderson and Ho, 1998; Cabrera et al., 1998; Gilbert et al., 2007). Similarly, the expression levels and distribution of ion channel, pump and exchanger proteins in myocytes are heterogeneous, giving rise to regional differences in action potential shape, duration, and conduction velocity (Boyett et al., 2009; Hucker et al., 2009; Nerbonne and Guo, 2002; Szentadrassy et al., 2005).

2.2.3. Extracellular matrix

Cardiac myocytes are surrounded and supported by the ECM, which is a complex network including strands of collagen and elastin. Both collagen and elastin are fibrous proteins, and their relative densities can vary with age, species, and tissue type (Abrahams et al., 1987; Ju and Dixon, 1996; Weber et al., 1994). For example, collagen is found in high densities throughout the ventricular myocardium, but is less abundant in papillary muscles and trabeculae. Moreover, the thickness of collagen fibrils can dramatically increase in pathological cases from 40 nm up to as much as 300 nm.

The arrangement of the ECM differs at specific locations (Robinson et al., 1983). In the endomysium, the collagen network surrounds a single myocyte, with interconnection to neighbouring myocytes. In the perimysium, bundles of perimysal collagen fibres envelop groups of adjacent myocytes and provide the laminar structure of the myocardium (Pope et al., 2008). Long perimysal collagenous tendons can link adjacent laminar structures. In the epimysium, collagen and elastin form a layer that is found at the epi- and endocardial surfaces.

2.2.4. Spatial organisation of fibroblasts

Fibroblasts form the largest population of cells in the heart, but their structural arrangement in cardiac tissue is still not well understood. It has been suggested that fibroblasts are organised in sheets that follow closely the structural arrangement of myocytes, with some fibroblasts forming strands that bridge cleavage planes between sheets (Goldsmith et al., 2004). Each myocyte is adjacent to several fibroblasts; in-vitro and in-situ studies have found evidence of functional gap junctions between fibroblasts and both myocytes and other fibroblasts (Kohl et al., 1994; Rook et al., 1992), suggesting that fibroblasts could play an active role in tissue electrophysiology (Kohl et al., 2005).

2.3. Micro-structural basis of bulk electrical properties

The spread of depolarisation through cardiac tissue depends on intercellular coupling through gap junctions, as well as intracellular and extracellular conductivities. Both intracellular and extracellular spaces are filled with conducting fluid and act as volume conductors, with low-resistance gap junctions connecting the intracellular spaces of adjacent cells. This structure ensures that the action potential upstroke in one part of the cell membrane results in depolarisation of neighbouring regions that is sufficient to open voltage-gated Na^+ channels in these regions, resulting in a propagating action potential (Jongsma and Wilders, 2000; Kleber and Rudy, 2004; Rook et al., 1992).

The electrical properties of bulk tissue depend on the conductivities of the intracellular and extracellular spaces. In general, both conductivities are anisotropic, and in turn depend on the relative volumes of myocytes and extracellular space, blood flow in the vasculature, myocyte shape and orientation, the distribution of gap junctions and their state, and the ionic composition of intracellular and extracellular spaces (Stinstra et al., 2005). Measuring these conductivities in tissue remains a challenge, because the properties listed above are either difficult to measure or vary regionally within the tissue. Estimating conductivities is further complicated by the different conditions under which experiments are carried out from one study to another. These difficulties explain the large range of experimentally measured values of intra- and extracellular conductivities and their anisotropy ratios as discussed in Section 4.3 (Roth, 1997; Stinstra et al., 2005). Macroscopic conductivities associated with fibroblasts are still not established and their role in determining bulk electrical properties is not well understood.

At the tissue level, measurements and quantitative description of conductivity is further complicated by the local orientation of fibres and, in ventricular tissue, sheets. Moreover, recent studies have shown that connexin43 expression can also vary throughout the ventricular wall (Poelzing et al., 2004). Optical mapping studies have examined how these macroscopic features affect conductivities by measuring space constants for membrane potential decay along and across fibres, following a sub-threshold stimulus (Akar et al., 2001; Poelzing et al., 2005).

3. Action potential propagation

Despite the complex structure described above, at the macroscopic scale cardiac tissue behaves as a functional syncytium, supporting propagating waves of depolarisation and repolarisation. The biophysics of this process has been reviewed extensively elsewhere (Kleber and Rudy, 2004; Plonsey and Barr, 2000). In this section we examine this continuum approximation and review the properties of action potential propagation in 1-, 2-, and 3-D.

3.1. Continuum approximation

At the cellular scale, there is a delay between the depolarisation of a myocyte and its neighbours that has been attributed to the effect of gap junctions. This is evidence that at this scale action potential propagation is a discrete process (Kleber and Rudy, 2004). However, at larger spatial scales depolarisation appears to propagate smoothly (Durrer et al., 1970). A common and important assumption underlying cardiac tissue electrophysiology is that in some cases the discrete nature of cardiac propagation may be neglected, and propagation can be considered as continuous, and this leads to a simplified mathematical description of the tissue (see Section 4). Support for this assumption comes from experiments in cultured neonatal rat ventricular cells. In 1-D strands of these cells with a single-cell thickness, gap junction delay was found to be around 118 μs, accounting for about half of the total conduction time. However, in strands containing several cell layers this delay was smaller and amounted to only 22% of the total conduction time (Fast and Kleber, 1993).

3.2. 1-D propagation

In the continuous limit, 1-D propagation is characterised by a single parameter, the conduction velocity (CV). This parameter is determined by many factors, the most important of them being membrane excitability (mainly depending on the magnitude of the fast Na^+ current, see Table 1) and the conductivities of cardiac tissue. Typical values of CV measured longitudinal to the cell axis are between 1.7 and 2.5 m s^{-1} in the conduction system, and between 0.48 and 0.61 m s^{-1} in the ventricles (Kleber and Rudy, 2004). Both lowering excitability and decreasing tissue conductivity result in reduction of CV and may therefore cause propagation block. CV also depends on the degree to which cardiac tissue has repolarised, and decreases as pacing cycle length shortens, a feature known as CV restitution. At cycle lengths of longer than about 1.5 times the action potential duration (APD), CV approaches a maximal saturated value. At shorter cycle lengths, CV usually decreases gradually because the depolarisation wavefront encounters tissue that has not fully repolarised. In some cases CV increases as cycle length is decreased. This phenomenon is called supernormality, and has been observed in Purkinje fibres, in some cardiac cell cultures, or under certain conditions (Chialvo et al., 1990; Endresen and Amlie, 1989; Endresen et al., 1987). The slope of the CV restitution curve is an important characteristic of myocardium, which is believed to influence the onset of dynamical heterogeneity in the heart (Mironov et al., 2008).

3.3. 2-D propagation

In 2-D, the 1-D features of cardiac action potential propagation are augmented by the effects of tissue anisotropy and wavefront curvature.

Anisotropic propagation results from the organisation of cardiac myocytes into fibres as described in Section 2. Longitudinal propagation along the principal axis of a fibre is faster than transverse propagation, resulting in axially symmetric anisotropy (Girouard et al., 1996). Since most gap junctions are located at the ends of myocytes, gap junction coupling in the transverse direction is limited (Hoyt et al., 1989). Both these factors contribute to anisotropy; however, a modelling study by Spach et al. (Spach et al., 2000) showed that myocyte shape is as important (or more so) as changes in gap junction distribution. Anisotropic propagation is characterised by two principal values of CV: a longitudinal CV parallel to fibres and a transverse CV orthogonal to fibres.

The second important characteristic of 2-D propagation is curvature. Fig. 4 displays three typical shapes of a wavefront: plane, convex and concave. The effects of curvature on wave propagation can be explained by the following simple arguments. A plane wavefront conserves its length locally and thus each depolarised cell needs to depolarise only one cell in front of it. In contrast the length of a convex wavefront steadily increases, and therefore the current initiating depolarisation spreads to a larger area than that for a plane front. As a result, convex fronts propagate more slowly than a plane front. Conversely, a concave front decreases its length during propagation, resulting in faster propagation. The dependency of velocity on curvature is an important factor determining normal and abnormal (re-entrant) wave propagation in cardiac tissue. Curvature effects are often also referred to as current-to-load or source-sink mismatch and may be important for propagation through Purkinje-muscle junctions.

Direct experimental measurement of the relationship between CV and curvature in real cardiac tissue remains difficult because of regional differences in CV and restitution (Nash et al., 2006; Yue et al., 2005), and because both curvature and anisotropy affect the velocity of wave propagation (Bernus et al., 2004). Fig. 5 shows an example of an indirect study of the curvature effects (Cabo et al., 1994), showing that the propagation velocity of a wave through a thin isthmus decreases as the isthmus width decreases. Numerical experiments performed by Cabo et al. confirmed that the decrease in velocity could largely be ascribed to the effect of wavefront curvature. They also showed that the radius of curvature of the wavefront could be estimated as half of the isthmus width. Therefore, the plot of dependency of velocity on the inverse isthmus width shown in Fig. 5 represents the influence of curvature on the velocity of wave propagation. Cabo et al. also found a particular size of the isthmus for which wave propagation was blocked, varying from 0.5 mm to 2.7 mm depending on the stimulation frequency. Based on these data, the minimal radius of a semicircular propagating wave is between 0.25 and 1.3 mm, and waves with a greater curvature cannot propagate. These figures are consistent with earlier estimates of 0.2 mm for critical radius, based on stimulation of cardiac tissue by electrodes of different sizes (Lindemans and Zimmerman, 1979).

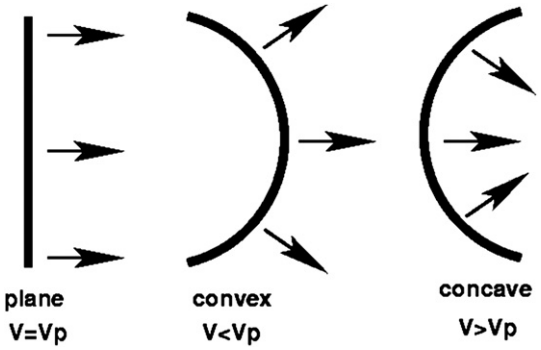

Fig. 4. Schematic representation of wave-front of different curvature and directions of local currents.

3.4. 3-D propagation

Propagation in 3-D is influenced by tissue anisotropy and curvature in a similar way to 2-D propagation. There is emerging evidence that 3-D propagation is modulated by the fibre-sheet structure of cardiac tissue (see Section 2.2.1), which extends axially symmetric anisotropic propagation with two principal values of CV to orthotropic propagation with three principal values of CV in the fibre direction, normal to fibre direction and in the sheet plane, and normal to the sheet plane. High-density intramural electrical mapping of active wave propagation in porcine ventricular tissue (Caldwell et al., 2009) has shown clear evidence of orthotropic propagation, with local conduction velocities of 0.67, 0.3, and 0.17 m s^{-1} in a ratio of 4.3:1.8:1.0 along the three main directions coinciding with the local micro-structure directions.

4. Mathematical description of cardiac tissue electrophysiology

Models of cardiac tissue electrophysiology encode information about excitability at the cell level and electrical conduction at the tissue level to enable quantitative description of action potential propagation. In discrete models the granular nature of cardiac tissue is characterised by an explicit representation of individual cells, whereas in continuous models cardiac tissue is treated as a functional syncytium. Both approaches involve a choice of parameters as well as a description of tissue geometry. In this section we review different types of cardiac tissue model, and discuss the choice of parameters and tissue geometry.

4.1. Models of discrete cardiac tissue

Mathematical descriptions of discrete cardiac tissue include simple cellular automaton (CA) models, coupled map lattices (CML) (Holden and Zhang, 1993), and lattices of coupled ordinary differential equations (or CODE lattice) (Winslow et al., 1993).

Cellular automata (CA) are simplified descriptions of cardiac tissue, in which each cell has a finite number of states. At each time step the state of each cell is updated to a new state that depends on its previous state and the state of its neighbours. This simplicity enabled CA models of cardiac action potential propagation to be formulated in mathematical terms (Wiener and Rosenblueth, 1946) and implemented on some of the earliest computers (Moe et al., 1964). CA updating rules have been developed to generate smoothly curved wavefronts that can take into account the effects of wavefront curvature described in Section 3.3 above (Bub et al., 2002; Gerhardt et al., 1990), and the effects of tissue anisotropy (Hall Barbosa, 2003). CA models are computationally cheap to implement, and have been used to examine the properties of spiral waves and in particular the effects of tissue heterogeneity (Bub et al., 2002; Greenberg and Hastings, 1978; Moe et al., 1964; Smith and Cohen, 1984). However, a major limitation of a CA approach is the discrete states that each cell can occupy, which makes it difficult to implement rate-dependent effects.

Coupled map lattices (CML) are a development of a CA approach in which states are continuous, but are updated by interactions within a lattice (Waller and Kapral, 1984). Each interaction can be allocated a different coupling strength, enabling anisotropic propagation to be modelled (Holden and Zhang, 1993).

A further refinement of the CML approach is to couple the ordinary differential equations (ODEs) describing the kinetics of an individual cell using resistors that represent gap junction connections. This type of model has been used to examine propagation in 1D fibres (Rudy, 1995; Shaw and Rudy, 1995, 1997b; Viswanathan et al., 1999) and 2D sheets (Winslow et al., 1993). A variant of this approach is to model cardiac tissue as a network of connected cables, which can be used to represent 3D tissue anisotropy (Vigmond and Leon, 1999). A particular strength of these approaches is that it is possible to construct detailed models of tissue architecture at the cell level, so that the effect of discrete gap junction conductances and cellular anisotropy can be studied (Roberts et al., 2008; Spach et al., 1992, 2000; Stinstra et al., 2006). However, without careful optimisation these approaches can be computationally expensive (Vigmond and Leon, 1999) and they also require description of cell size and capacitance, the composition of the extracellular space, as well as data on the location and conductance of individual gap junctions.

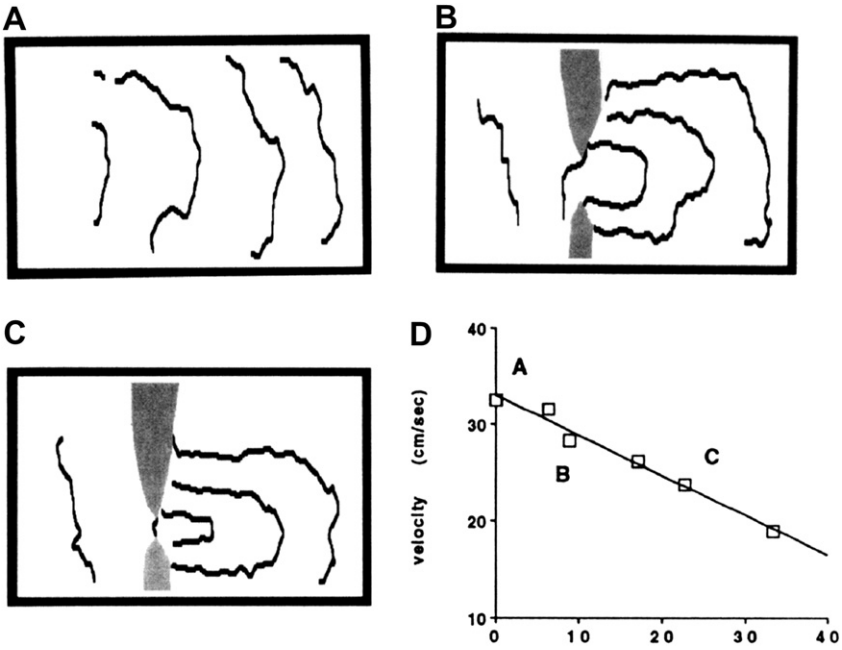

Fig. 5. Relation between the isthmus width and the velocity of the wavefront. Experiments in sheep myocardium. Fibres are directed horizontally. Isochronal maps before creation of the isthmus (A) and for isthmus widths of 2.26 mm (B) and 0.88 mm (C). D conduction velocity vs inverse isthmus width. Reproduced from (Cabo et al., 1994) with permission.

4.2. Continuous approximation of cardiac tissue

At the tissue scale cardiac tissue behaves as a functional syncytium of electrically coupled cells (Section 3.1). A homogenisation of the discrete representation of cardiac tissue as a resistor network can be applied to derive a continuous description (Neu and Krassowska, 1993), and its idealised electrical behaviour may be considered as an excitable medium in 1-, 2-, or 3-D, where excitable cells are coupled diffusively via transmembrane voltage V_m (Keener and Sneyd, 1998)

4.2.1. Bidomain model

Bidomain models represent cardiac tissue as a syncytium composed of intracellular and extracellular domains. It is assumed that both domains are overlapping and continuous, but separated by the cell membrane. The bidomain model of cardiac tissue is based on current flow, distribution of electrical potential and the conservation of charge and current (Henriquez, 1993).

The description of each domain is based on a generalised version of Ohm's law defining the relationship between the electric field $\mathbf{E}$ (in V m^{-1}) derived from the potential ϕ(V), the current density $\mathbf{J}$ (A m^{-2}), and the conductivity tensor $\mathbf{G}$ (S m^{-1}):

$$\begin{aligned} \mathbf{E} &= -\nabla\phi \\ \mathbf{J} &= \mathbf{G}\,\mathbf{E} = -\mathbf{G}\,\nabla\phi \end{aligned} \tag{1}$$

Considering the intracellular and extracellular spaces specifically, we have:

$$\begin{aligned} \mathbf{J}_i &= -\mathbf{G}_i\nabla\phi_i \\ \mathbf{J}_e &= -\mathbf{G}_e\nabla\phi_e \end{aligned} \tag{2}$$

Where $\mathbf{J}_i$ and $\mathbf{J}_e$ are the intra- and extracellular current densities, $\mathbf{G}_i$ and $\mathbf{G}_e$ are intra- and extracellular conductivity tensors respectively, and ϕ_i and ϕ_e are the electrical potential in the intracellular and extracellular spaces.

Considering the conservation of current and charge, and assuming only membrane related sources in the intra- and extracellular spaces we can write divergence equations:

$$\begin{aligned} \nabla\cdot\mathbf{J}_i &= -I_m, \quad \nabla\cdot\mathbf{J}_e = I_m \\ \nabla\cdot(\mathbf{J}_i+\mathbf{J}_e) &= 0, \end{aligned} \tag{3}$$

where I_m (A m^{-3}) is transmembrane current per unit volume, which is composed of a capacitive component with units A m^{-2} and an ionic component i_{ion} resulting from current flow through ion channels, pumps and exchangers in the cell membrane, with units A m^{-2}.

$$I_m = \beta_m\left(C_m\frac{\mathrm{d}V_m}{\mathrm{d}t}+i_{ion}\right), \tag{4}$$

Here β_m (m^{-1}) is the surface area-to-volume ratio of a cardiac cell, C_m (F m^{-2}) the specific cell membrane capacitance, and V_m the transmembrane voltage, which is given by:

$$V_m = \phi_i - \phi_e \tag{5}$$

Combining Equations (2)–(5), we obtain:

$$\begin{aligned} \nabla\cdot\mathbf{G}_i(\nabla V_m+\nabla\phi_e) &= \beta_m\left(C_m\frac{\partial V_m}{\partial t}+i_{ion}\right) \\ \nabla\cdot((\mathbf{G}_i+\mathbf{G}_e)\nabla\phi_e) &= -\nabla\cdot(G_i\nabla V_m) \end{aligned} \tag{6}$$

Equation (6) represents the bidomain model of cardiac tissue. Assuming that the extracellular space is bounded and there is no electric current flowing from the extracellular space to adjacent spaces homogeneous Neuman (no-flux) boundary conditions can be implemented at the boundary Γ as:

$$\begin{aligned} \Gamma: &\quad \mathbf{n}\cdot(\mathbf{G}_i\nabla\phi_i) = \mathbf{n}\cdot(\mathbf{G}_i\nabla(V_m+\phi_e)) = 0 \\ \Gamma: &\quad \mathbf{n}\cdot(\mathbf{G}_e\nabla\phi_e) = 0, \end{aligned} \tag{7}$$

where $\mathbf{n}$ is the outward normal to the boundary Γ.

The conductivity tensors in Equation (5) ($\mathbf{G}_i$ and $\mathbf{G}_e$) are determined by the anisotropy of cardiac tissue, and their components depend on the tissue conductivities as well as the local orientation of tissue within the coordinate system of the model.

4.2.2. Monodomain model

The bidomain model of cardiac tissue (Equation (6)) can be simplified by assuming that the anisotropy of the intracellular and extracellular spaces is the same, i.e. that the conductivity in the extracellular space is proportional to the intracellular conductivity:

$$\mathbf{G}_e = \lambda\mathbf{G}_i \tag{8}$$

where λ is a scalar, representing the ratio between the conductivity of the intra- and extracellular spaces.

Substituting equation (8) into equation (6), we have:

$$\nabla\cdot\frac{\lambda}{1+\lambda}\mathbf{G}_i\nabla V_m = \beta_m\left(C_m\frac{\partial V_m}{\partial t}+i_{ion}\right) \tag{9}$$

If we introduce an effective conductivity $\mathbf{G} = (\lambda)/(1+\lambda)\mathbf{G}_i$, we obtain the monodomain model of cardiac tissue as:

$$\nabla\cdot\mathbf{G}\,\nabla V_m = \beta_m\left(C_m\frac{\partial V_m}{\partial t}+i_{ion}\right), \tag{10}$$

With the no-flux boundary condition:

$$\Gamma: \quad \mathbf{n}\cdot(\mathbf{G}\,\nabla V_m) = 0 \tag{11}$$

The monodomain equation (10) is often written as.

$$\frac{\partial V_m}{\partial t} = \nabla\cdot\mathbf{D}\nabla V_m - \frac{i_{ion}}{C_m} \tag{12}$$

where $\mathbf{D}$ (m^2 s^{-1}) is a diffusion tensor or scalar diffusion coefficient. In the case of axially symmetric anisotropy, where diffusion in all directions orthogonal to the fibre direction is assumed to be the same, propagation is described by two values of the diffusion coefficient; a longitudinal coefficient D_1 for propagation along fibres, and a transverse coefficient D_2 for propagation orthogonal to the fibres. If the fibre direction is given by the vector $\mathbf{f}$, the diffusion tensor can be written:

$$\mathbf{D} = D_2\mathbf{I} + (D_1 - D_2)\mathbf{f}\mathbf{f}^T \tag{13}$$

where $\mathbf{I}$ is the identity matrix, and $\mathbf{f}^T$ is the transpose of $\mathbf{f}$. The elements of $\mathbf{D}$ can be written as follows (Panfilov and Keener, 1995):

$$d_{ij} = \begin{cases} D_2 + (D_1 - D_2)f_if_j & (i = j) \\ (D_1 - D_2)f_if_j & (i \neq j) \end{cases} \tag{14}$$

For orthotropic anisotropy with principal directions longitudinal to fibres in the sheet plane, normal to fibres in the sheet plane, and normal to the sheet plane, the diffusion tensor is given by (Colli-Franzone et al., 2005):

$$\mathbf{D} = D_1\mathbf{f}\mathbf{f}^T + D_2\mathbf{s}\mathbf{s}^T + D_3\mathbf{n}\mathbf{n}^T \tag{15}$$

where D_1, D_2 and D_3 are diffusion coefficients longitudinal to fibres, normal to fibres in the sheet plane, and normal to both fibres and sheets, and $\mathbf{f}$, $\mathbf{s}$ and $\mathbf{n}$ are unit vectors in the corresponding directions. Since $\mathbf{f}$, $\mathbf{s}$ and $\mathbf{n}$ are orthonormal

$$\mathbf{ff}^T + \mathbf{ss}^T + \mathbf{nn}^T = \mathbf{I}, \tag{16}$$

where $\mathbf{I}$ is the identity matrix. Hence equation (15) can be rewritten as

$$\mathbf{D} = \mathbf{D}_2 I + (D_1 - D_2)\mathbf{ff}^T + (D_3 - D_2)\mathbf{nn}^T, \tag{17}$$

which reduces to equation (13) for axially symmetric anisotropy where $D_3 = D_2$.

4.2.3. Comparison between bidomain and monodomain models

If there is no injection of current into the extracellular space, descriptions of action potential propagation provided by monodomain and bidomain models are close to each other even under the condition of unequal anisotropy ratio in the extracellular and intracellular spaces (Colli-Franzone et al., 2005). A recent study (Potse et al., 2006) compared patterns of action potential propagation simulated using monodomain and bidomain models. They found that in the absence of external stimuli, the patterns obtained with the monodomain model were almost identical to those obtained with a bidomain model. Similarly, Roth examined spiral wave tip trajectories in monodomain and bidomain models and found that in most cases the trajectories were similar in both cases (Roth, 2001). The monodomain model is a single PDE, and numerical solutions are easier to obtain (see Section 6). However, the bidomain model provides a more detailed description of cardiac tissue, and the separation of intracellular and extracellular spaces is necessary to accommodate the injection of current into the extracellular space during external stimulation and defibrillation (Trayanova, 2006). During defibrillation, the unequal anisotropy of the intracellular and extracellular spaces plays an important role in generating *virtual electrodes* that are essential for successful defibrillation (Wikswo et al., 1995). The bidomain model can be expanded to include further domains, and one example of this approach is a model that includes an additional domain representing fibroblasts (Sachse et al., 2009).

4.3. Parameters

The key parameters that determine the conduction properties of a tissue model are elements of the effective diffusion tensor or the diffusion coefficient, which in turn depend on the tissue conductivities, surface-to-volume ratio and specific capacitance (Winfree, 1998).

As described in Section 2.3, the intracellular and extracellular conductivities are determined by the local tissue micro-structure and the composition of the intracellular and extracellular spaces, which vary within the tissue and are further modified by local blood flow. Measurements of longitudinal conductivity span the range of 0.17–0.45 Sm^{-1} for intracellular space, and 0.12–0.62 Sm^{-1} for extracellular space; corresponding measurements for transverse conductivity range from 0.019 to 0.06 Sm^{-1} for intracellular space and 0.08–1.74 Sm^{-1} for extracellular space (Stinstra et al., 2005). Typically, the values for conductivities chosen for simulation studies lie within these ranges, and result in a plausible CV (Colli-Franzone et al., 2005). However, detailed models of cardiac micro-structure developed with the purpose of reconstructing the effect of cardiac micro-structure on conductivity indicate that there may not be definitive values of conductivity, but rather a range of typical values with local variation (Stinstra et al., 2005).

Experimental measurements of surface-to-volume ratio range from 2400 to 8900 cm^{-1} depending on species and developmental stage (Bers, 2008). Typical values chosen for tissue models range from 1000 to 5000 cm^{-1} (Colli-Franzone et al., 2005; Keener and Bogar, 1998; TenTusscher et al., 2004; Xu and Guevara, 1998), which for an idealised cylinder correspond to a value of around 2 divided by the cell radius (Winfree, 1998).

Specific membrane capacitance is usually measured to be in the range 1–10 $\mu F\ cm^{-2}$. This value combined with typical values of conductivities and cellular dimensions gives CV within the physiological range. The membrane capacitance of the squid giant axon was estimated to be about 1 $\mu F\ cm^{-2}$ based on measurements of the time course of membrane current following a sub-threshold voltage step (Curtis and Cole, 1938). However, similar studies in cardiac Purkinje fibres yielded a higher value of around 10 $\mu F\ cm^{-2}$ (Fozzard, 1966; Schoenberg et al., 1975). This higher value can be attributed to two components of the membrane capacitance, a surface component associated with the outer sarcolemma and a deep component associated with clefts in the cell membrane (Fozzard, 1966). The cleft capacitance charges only slowly, and so is thought to make only a small contribution to action potential propagation. Since about 90% of the ventricular cell membrane is located within clefts and the t-tubule system, a specific membrane capacitance of 1 $\mu F\ cm^{-2}$ is justified (Noble, 1979) although some tissue models have used a higher value of 2 $\mu F\ cm^{-2}$ (TenTusscher et al., 2004).

A common approach taken to determine suitable parameter values for a computational model is to vary the conductivities (or diffusion coefficients) to ensure that CVs within the observed range are achieved. However, because these parameters have an important effect not only on CV but also on features such as conduction block, a more rigorous approach based on experimental work is needed to determine the range of suitable values and how, for example, these are modified by disease processes.

4.4. Tissue geometries and imaging data

Models of cardiac tissue can be implemented with either idealised geometries (1-D strand, 2-D sheet or 3-D box), or anatomically detailed geometries based on reconstructions from dissection or imaging data (2-D slice, 3-D slab or whole organ). A simplified geometry enables propagation to be studied in the absence of anatomical detail, whereas more detailed geometrical models with high spatial resolution enable the role of anatomical structures to be evaluated.

Based on various experimental techniques that include histology, confocal microscopy, magnetic resonance imaging (MRI) and diffusion tensor MRI (DT-MRI), realistic anatomic structures of cardiac tissue with high spatial resolutions have been reconstructed for single myocytes (Savio-Galimberti et al., 2008), the sino-atrial node (Dobrzynski et al., 2005), atrial tissue (Lasher et al., 2009), the whole atrium (Seemann et al., 2006), and ventricle (Hsu et al., 1998; Nielsen et al., 1991). Furthermore anatomically detailed models of canine (Nielsen et al., 1991), rabbit (Vetter and McCulloch, 1998), pig (Stevens and Hunter, 2003) and mouse (Sampson and Henriquez, 2005) ventricular anatomy defined on a finite-element mesh have been constructed, as well as highly detailed models of small portions of ventricular tissue imaged at spatial resolutions of around 1 μm (Pope et al., 2008; Sands et al., 2005). Whole ventricle anatomical models combining histology data at resolutions of around 20 μm with MRI data at a resolution of 100 μm are being developed (Gilbert et al., 2009; Plank et al., 2009), along with whole heart models using MRI data at a resolution of 120 μm (Cherry and Fenton, 2008).

Diffusion tensor MRI (DT-MRI) provides a non-invasive tool to reconstruct the anatomical structures and fibre orientation of cardiac tissue, especially in the ventricles. This technique measures the Brownian motion of protons, which reflects to some extent the fibre structure of the tissue because the motion of protons is constrained by the cell membrane. The use of this approach for ventricular tissue has been validated by its correlation with histological data (Holmes et al., 2000; Hsu et al., 1998; Scollan et al., 2000). DT-MRI provides a diffusion tensor with its primary eigenvector being correlated to cardiac fibre orientation, whilst the

secondary and tertiary eigenvectors being have been proposed to relate to the orientation of cardiac sheets (Helm et al., 2005). However, the typical spatial resolution available with DT-MRI may not be sufficient to correctly identify the sheet structure in ventricular tissue because there may be more than one sheet orientation within the volume of tissue that produces the DT-MRI signal (Gilbert et al., 2007).

At the cell scale there are often discontinuities in tissue structure, especially at the junctions between two distinctive tissue regions, such as at the junction of the crista terminalis and the pectinate muscle in the right atrium, the junction of the right ventricular free wall and ventricular septum, and Purkinje-ventricular junctions. At these locations fibre orientation changes abruptly, and these changes not only complicate the process of obtaining a mesh from DT-MRI data, but may also require special numerical treatment.

5. Integration of cell and tissue models of cardiac electrophysiology

As described above, models of tissue electrophysiology integrate individual cells together into a given structure, where each cell is electrically connected to multiple neighbours. The coupling between cells is generally represented as a diffusive process, which gives rise to an electrotonic (diffusive) current between neighbouring cells. This electrotonic current can modify cellular electrophysiology both quantitatively and qualitatively in both real tissue and models. In this section, we present some of the issues associated with simulating cardiac tissue electrophysiology and discuss their implications.

5.1. Emergent properties in tissue

When individual cells are coupled together to form tissue, new properties that have no single-cell equivalents emerge. In this section we describe some of these fundamental properties and discuss their importance to tissue behaviour.

5.1.1. Liminal length

In a single cell, an action potential can be elicited from a stimulus provided the stimulus current has sufficient magnitude and duration to raise the membrane potential above its threshold of excitability. In tissue, neighbouring cells that are initially polarised act as current sinks and so counteract a stimulus current. Thus, enough current must be injected to raise the membrane potential of neighbouring cells above threshold, while also ensuring that the membrane potential at the stimulus site is not decreased below threshold by electrotonic current flow to polarised neighbours. This requirement introduces a new spatial scale to the stimulation process; a large enough region of tissue must be stimulated directly for a wave to develop and propagate. Although the length (in 1-D) necessary to initiate propagation depends on the magnitude and duration of the injected current, there is a minimum length below which no combination of stimulus strength and duration can produce a propagating wave. This minimum length is called the *liminal length*, which in cardiac tissue is typically of the order of 1 mm (Fozzard and Schoenberg, 1972; Noble, 1972; Rushton, 1937). The corresponding concepts of liminal area and liminal volume apply in 2- and 3-D, respectively. Stimulating a region of size below the liminal length (or area or volume) ensures that the stimulus will dissipate without producing a propagating wave, even if the same magnitude and duration of the stimulus current successfully elicits an action potential in a single cell with the same electrophysiological characteristics. This concept is related to the safety factor for propagation (Kleber and Rudy, 2004; Shaw and Rudy, 1997a). Because different models may have different thresholds of excitability, liminal length is a model-dependent property.

5.1.2. Minimum cycle length for propagation

Another important property associated with excitable tissue is the appearance of a minimum cycle length that can be used to achieve successful wave propagation. This is also known as the effective refractory period (ERP). In a single cell, any stimulus current causes a change of the membrane voltage, even within the refractory period. However, in tissue a response may occur at the site of stimulation, but neighbouring tissue within the refractory period will not be able to sustain a wave, and propagation will fail. As tissue is paced faster, there is less recovery time before the next beat, so that there is a minimum cycle length at which the tissue can be paced and below which propagation failure occurs. As an example, Fig. 6 shows the minimum cycle length for propagation in tissue compared to the minimum cycle length achievable in a single cell (using a stimulus current magnitude of twice diastolic threshold) for the Nygren et al. model for human atrial cells (Nygren et al., 1998) and the Fox et al. model for canine ventricular cells (Fox et al., 2002). It is possible to pace the Nygren et al. model at extremely short cycle lengths in a single cell, whereas when embedded in a tissue model propagation fails for cycle lengths below 320 ms. Similarly, the Fox et al. model can be paced at a minimum cycle length of 90 ms for a single cell, but propagation fails for cycle lengths below 190 ms in a tissue model. Because the diastolic interval characterises the recovery time following an action potential, the minimum cycle length for propagation is associated with the minimum diastolic interval for propagation. This important property of real tissue may not be captured by simplified or generic models (see Section 6).

5.1.3. Conduction velocity

With the introduction of propagation in tissue, the property of CV emerges. CV is related to the strength of cell-to-cell coupling, and scales as the square root of the diffusion coefficient D (see equation (12)). CV is also determined by the characteristics of the action potential upstroke. Although the maximum upstroke velocity (maximum dV_m/dt) is loosely correlated with maximum CV, it is not especially useful as a velocity predictor, as can be seen

Table 1
Maximum conduction velocity (CV_{max}), maximum upstroke velocity (dv/dt_{max}), and maximum conductance sodium current (g_{Na}) in tissue for 14 different models, in order of decreasing CV_{max}. Although overall CV_{max} and g_{Na} decreases as dv/dt_{max} decreases, neither value can be used alone to predict CV_{max}. The value of g_{Na} is not available for the Nygren et al. model because it uses the Goldman-Hodgkin-Katz formulation for I_{Na} that uses membrane permeability rather than conductance. In all cases, the explicit Euler method is used with a spatial resolution of 0.01 cm, time step of 0.01 ms, and diffusion coefficient of 0.001 cm^2/ms. CV and dv/dt_{max} are measured at the center of a 1 cm-long cable paced at a cycle length of 1000 ms.

Model	Reference	CV_{max} (cm/s)	dv/dt_{max} (V/s) in tissue	g_{Na} (nS/pF)
Luo-Rudy I	(Luo and Rudy, 1991)	64.7	275	23
Shannon et al.	(Shannon et al., 2004)	61.8	263	16
Iyer et al.	(Iyer et al., 2004)	60.1	266	56.32
Faber-Rudy	(Faber and Rudy, 2000)	59.4	246	16
ten Tusscher et al.	(TenTusscher et al., 2004)	59.4	227	14.838
Priebe-Beuckelmann	(Priebe and Beuckelmann, 1998)	58.7	247	16
Mahajan et al.	(Mahajan et al., 2008)	52.2	172	12
Fox et al.	(Fox et al., 2002)	51.3	196	12.8
Courtemanche et al.	(Courtemanche et al., 1998)	50.4	127	7.8
Beeler-Reuter	(Beeler and Reuter, 1977)	47.6	110	4
Hund-Rudy	(Hund and Rudy, 2004)	47.3	133	8.25
Pandit et al.	(Pandit et al., 2001)	45.1	103	8
Nygren et al.	(Nygren et al., 1998)	39.5	83	n/a
Bondarenko et al.	(Bondarenko et al., 2004)	39.1	94	13

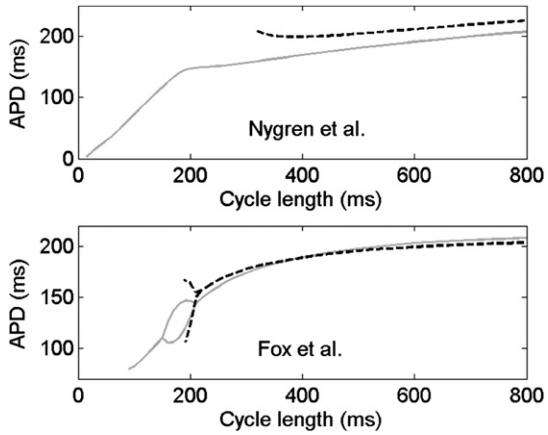

Fig. 6. Rate adaptation plots show the minimum cycle length for propagation in tissue compared to the minimum cycle length in a single cell. For a stimulus amplitude twice diastolic threshold, much smaller cycle lengths can be achieved in single cells (grey, solid) than in tissue (black, dashed) because action potentials do not always propagate in tissue. Dynamical properties therefore can be significantly different in tissue, as in the Fox et al. model, where the range of cycle lengths exhibiting alternans is reduced in tissue and no return to the 1:1 response at short cycle lengths is observed.

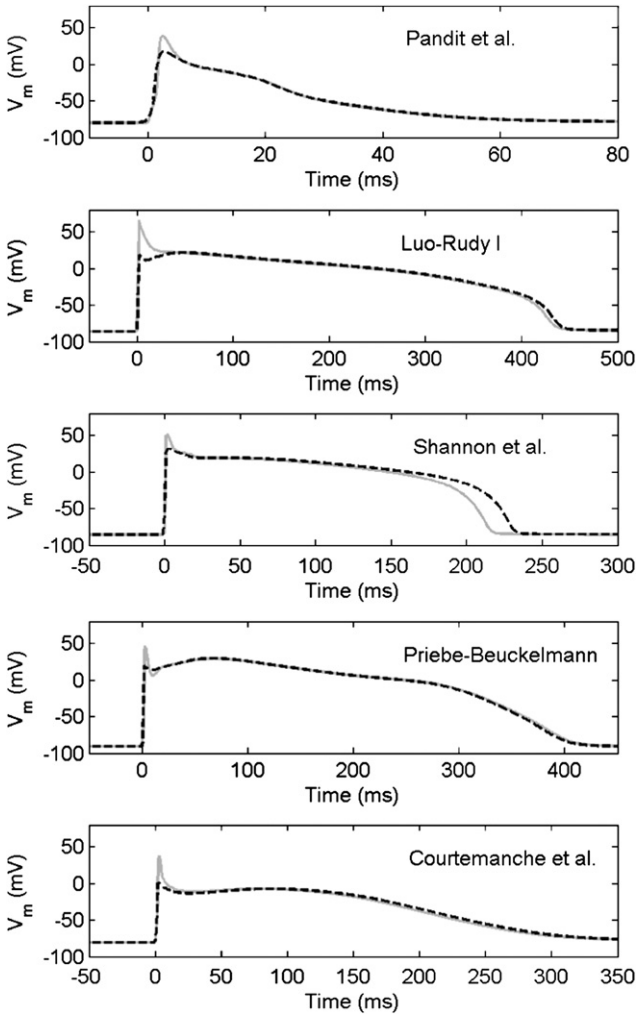

Fig. 7. Effects of cell coupling on action potential amplitude. In single cells (grey, solid), depolarizing current is applied directly to the cell. In tissue away from the stimulus site (black, dashed), the stimulating current is mediated through the electrotonic current coupling neighbouring cells. Because the electrotonic current includes contributions from neighbours not yet depolarised, action potential amplitudes in tissue are generally smaller than those in single cells. Action potentials are shown for a cycle length of 500 ms for the Pandit et al. and Shannon et al. models and for a cycle length of 1000 ms for the Luo-Rudy I, Priebe-Beuckelmann, and Courtemanche et al. models.

in Table 1. For example, the CV obtained for the Fox et al. model for canine ventricular cells (Fox et al., 2002) is only 8 percent larger than that obtained with the Hund-Rudy model for canine ventricular cells (Hund and Rudy, 2004); however, maximum dV_m/dt for the Fox et al. model is 47 percent larger than that of the Hund-Rudy model. Similarly, the CV obtained using the ten Tusscher et al. model for human ventricular cells (TenTusscher et al., 2004) is the same as the CV obtained with the Faber-Rudy model of guinea-pig ventricular cells (Faber and Rudy, 2000), with a dV_m/dt_{max} that is 8 percent smaller; and the CVs of the Nygren et al. (Nygren et al., 1998) and Bondarenko et al. (Bondarenko et al., 2004) models differ by only 1 percent, although dV_m/dt_{max} is 13 percent larger for the Bondarenko et al. model. In addition, the CV of the Courtemanche et al. model for human atrial cells (Courtemanche et al., 1998) is 7 percent larger than that of the Hund-Rudy model, whereas maximum dV_m/dt is actually 5 percent smaller for the Courtemanche et al. model. The value of maximum dV_m/dt has been shown to depend not only on membrane kinetics but also on electrotonic currents from neighbouring cells (Spach et al., 1992). CV also is correlated loosely with the maximum Na^+ conductance g_{Na}, with exceptions such as the relatively high conductance values for the Iyer et al. (Iyer et al., 2004) and Bondarenko et al. (Bondarenko et al., 2004) models and the relatively low value for the Beeler-Reuter model (Beeler and Reuter, 1977).

5.2. Electrotonic current-mediated differences in dynamics

The flow of current within the tissue resulting from regional differences in potential can have an important influence on local dynamics and excitation.

5.2.1. Decreased action potential amplitude and shape

When an action potential propagates in tissue, cells outside the stimulus region are brought above the excitability threshold purely through electrotonic currents from neighbouring depolarised cells. In addition, neighbouring cells that have not yet been depolarised remove current from cells that are beginning to depolarise. As a result, the action potential amplitude in tissue is generally reduced compared to the amplitude in single cells (or in tissue regions where a stimulating current is injected directly). Fig. 7 shows decreased action potential amplitude in tissue compared to single cells for five different models (Courtemanche et al., 1998; Luo and Rudy, 1991; Pandit et al., 2001; Priebe and Beuckelmann, 1998; Shannon et al., 2004). Amplitude reductions of up to 20% have been observed in models (Bueno-Orovio et al., 2008).

The effects of reduced action potential amplitude can have significant consequences. Fig. 8 shows how reduced action potential amplitudes in tissue can affect transmembrane currents and the overall action potential morphology and duration. In this case, the reduction in amplitude leaves the maximum voltage attained outside the stimulus region below the threshold for activation of the L-type Ca^{2+} current. As a result, the action potential plateau develops later and in a different manner, resulting in action potential prolongation away from the stimulus site.

Experimental and modelling studies have shown that electrotonic current can affect the shape of the action potential. One study (Conrath et al., 2004) showed that in some models of cardiac tissue the duration of propagating action potential is up to 80 ms shorter than action potential duration in uncoupled cells. Moreover, earlier experimental studies on dog hearts showed that the repolarisation

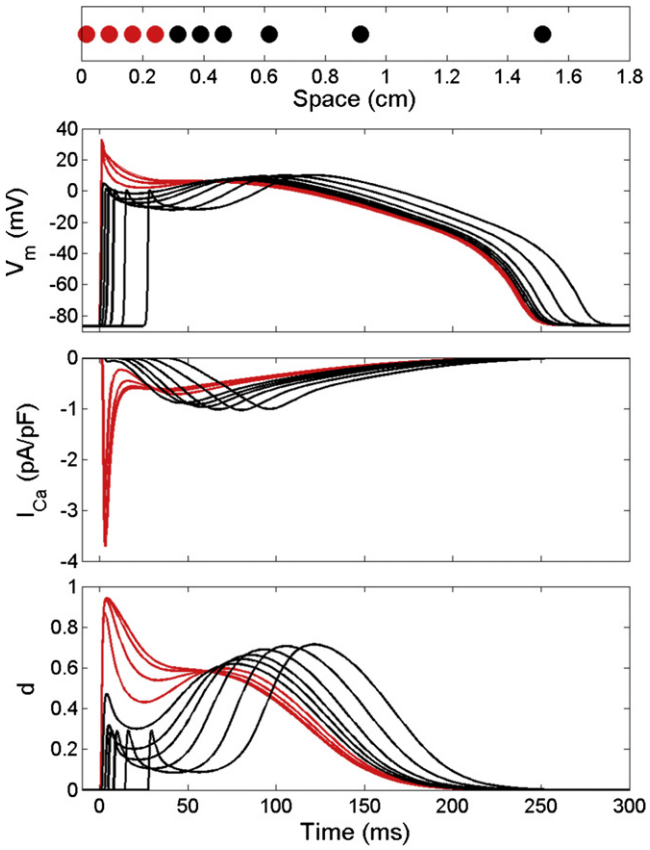

Fig. 8. Effect of the decrease in action potential amplitude in tissue on action potential morphology. Within the region directly stimulated (red traces from red locations indicated at top), the action potential retains a large amplitude, but the amplitude is decreased by more than 35 mV outside the stimulated region (black traces from black locations indicated at top). As a result, the L-type calcium current ($i_{Ca,L}$) is not activated normally outside the stimulus region because the voltage V_m is insufficient to open the *d*-gate. Hund-Rudy model (Hund and Rudy, 2004) in a 1.8-cm-long cable with the stimulus applied within the first 0.3 cm.

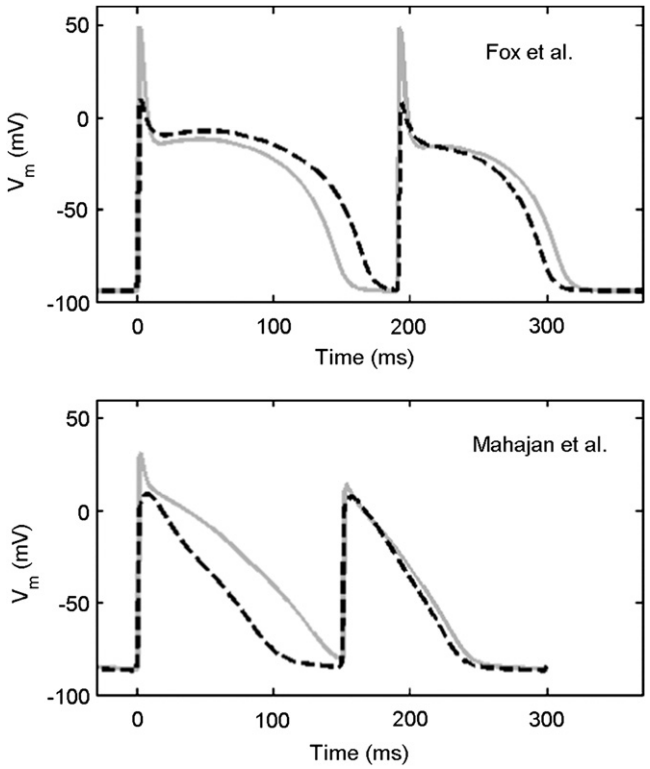

Fig. 9. Differences in alternans magnitude between single cells (grey, solid) and tissue (black, dashed). In the Fox et al. model, the alternans increases in tissue, while in the Majahan et al. model, the alternans magnitude decreases. Cycle lengths shown are 190 ms for the Fox et al. model and 150 ms for the Mahajan et al. model.

phase of the action potential can be modulated by the activation sequence or distance from pacing site (Abildskov, 1976; Osaka et al., 1987). The APD was found to progressively decrease as the wave moved away from the stimulation site, and this effect was more pronounced in directions transverse to the local fibre orientation (Osaka et al., 1987). Evidence of this negative linear correlation between APD and activation time has been found in several animal species including humans (Hanson et al., 2009). However, the amount by which APD decreases as a function of activation time may be species-dependent due to different expressions of ionic currents underlying the repolarisation phase, as recently suggested in a computational study by Sampson and Henriquez (Sampson and Henriquez, 2005).

5.2.2. Changes in restitution, alternans, and memory

Restitution is the rate adaptation of cardiac cells and tissue, alternans is beat to beat alternation in action potential shape and duration, and memory is the extent to which a particular action potential depends on the sequence of preceding beats. In tissue, a number of important dynamical properties associated with restitution, alternans, and memory may be altered by the presence of electrotonic currents. Fig. 9 shows an example of how alternans properties can change in tissue. For the Fox et al. model (Fox et al., 2002), the magnitude of alternans (difference between long and short APDs for one cycle length) is increased in tissue, but 2:1 block occurs at a relatively long cycle length, thereby reducing the range of cycle lengths over which alternans is experienced. For the Mahajan et al. model (Mahajan et al., 2008), the alternans magnitude is decreased in tissue over range of cycle lengths that experience alternans. A number of differences in other properties, including restitution curve shape and slope, alternans onset cycle length and magnitude, and memory amplitude, have been described in detail (Bueno-Orovio et al., 2008; Cherry and Evans, 2008; Cherry and Fenton, 2007; Cherry et al., 2008; Nygren et al., 1998; Ten Tusscher et al., 2006).

Electrotonic effects can influence not only the presence and characteristics of alternans but also on the stability of re-entrant waves. As an example, Fig. 10 shows the Fox et al. model in two cases: the original parameter set and with the conductance g_{Kr} doubled. Doubling g_{Kr} eliminates alternans in a single cell; however, electrotonic effects cause the alternans to reappear in tissue, similar to the case with original parameter values. In 2-D, the original parameters give rise to a stable spiral wave, whereas doubling g_{Kr} leads to sustained spiral wave breakup from the same initial conditions. The output of models that are intended to be predictive should therefore be interpreted carefully. Interventions that appear promising in single cells may not produce the same results in tissue, and indeed may lead to less desirable electrophysiological behaviour.

6. Numerical implementation of cardiac tissue models

This section addresses numerical issues related to modelling of cardiac tissue electrophysiology; in particular we discuss discrete space and discrete time representations of the continuous

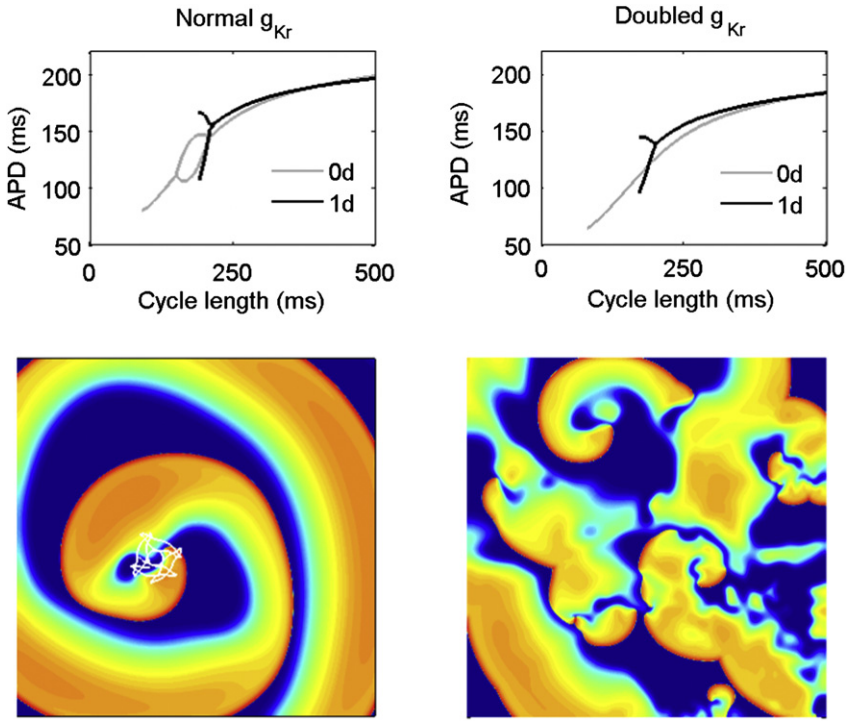

Fig. 10. Differences in dynamics between the Fox et al. model with original parameters and a modification where the maximal conductance g_{Kr} is doubled. With the modification, alternans is eliminated in a single cell (0-D) but reappears in tissue (1-D), and a spiral wave initiated in two-dimensional tissue experiences sustained breakup. 2-D domain is 30 cm × 30 cm; both spiral wave simulations are shown after 6.3 s of simulation time.

bidomain and monodomain equations and the types of mesh used to represent tissue geometry. Furthermore, we provide an overview of the techniques used for numerical simulations of tissue electrophysiology.

6.1. Modelling approaches

As described earlier, models of cardiac tissue electrophysiology are based on reaction–diffusion-systems where the reaction process is attributed to the cellular action potential, and the diffusion process represents current flow between cells. Most modelling approaches including mono-, bi-, or multidomain models assume that cardiac tissue behaves as a functional syncytium (Henriquez and Papazogou, 1996; Sachse et al., 2009), and the numerical implementations discussed in this section are related to these approaches.

6.2. Discrete representations of tissue geometry

Discrete models of tissue geometry can be constructed in various ways. Standard spatial models include 2- and 3-D tissue segments, ventricles and whole heart geometries. These models are commonly composed of discrete volume elements, for example tetrahedra (Bourgault et al., 2003; Vigmond et al., 2002) and hexahedra (Colli Franzone and Pavarino, 2004; Seemann et al., in press). Each element type has advantages and disadvantages. For instance, a mesh assembled from uniform cubic voxels can be derived easily from imaging data, but does not reconstruct curved surfaces such as the epicardium effectively. In contrast, irregular tetrahedral meshes can improve the representation of surfaces, but mesh generation can be more difficult and the numerical methods associated with irregular meshes can result in higher computational costs.

Common approaches are to construct a regular mesh with uniform elements, or an irregular mesh with elements of uniform type, but different shape and size. Hybrid meshes, with uniform and non-uniform elements used to represent less important regions, and grid refinement at critical points, border zones or at areas of large gradients in physical fields have been considered. Meshes that accurately represent complicated tissue anatomy while meeting the requirements of computational methods are difficult to construct, and this area remains an important challenge. Various mesh generation tools have been developed in other engineering fields, and some of these tools may be useful for generating models of tissue geometry. Recent work aims at providing meshes with high spatial accuracy that are appropriate for the computational methods used in simulation of tissue electrophysiology (Prassl et al., 2009). Adaptive mesh generation during the simulation has also been suggested to decrease calculation time (Deuflhard et al., 2009) (see Section 7.4).

6.3. Numerical methods for discrete space

The bidomain (equation (6)) and monodomain (equations (10) and (12)) models are based on Ohm's law and Poisson's equation for stationary electrical currents. In this section, we will focus on numerical approaches for solving Poisson's equation, which allow for a sound description of the anisotropic electrical properties of cardiac tissue. Mathematically, Poisson's equation is a set of partial differential equations (PDEs), and analytical solutions exist only for special cases. In general, numerical techniques implemented on computers are used for solving these PDEs. To approximate the PDEs, they are transformed into linear systems of equations (LSE) of the form $Ax + b = 0$ using discretisation techniques. In cardiac electrophysiology, the Finite Difference Method (FDM), the Finite Volume Method (FVM) and the Finite Element Method (FEM) are the most commonly applied techniques to transform Poisson's equation into LSEs. Less often, the Boundary Element Method, mesh free methods, and spectral methods have been used (Bueno-Orovio et al., 2006; Chinchapatnam et al., 2009; Fischer et al., 2000).

The FDM is based on approximating the partial derivatives of PDEs by difference quotients. The underlying spatial mesh is usually structured, so for example in 3-D the mesh consists of uniform cubic voxels. The FDM has been applied by many groups over many years for studies of tissue electrophysiology, for examples see (Potse et al., 2006; Pullan et al., 2005; Seemann et al., in press). This approach can be generalised for grids with irregular spacing (Trew et al., 2005b). The advantage of the FDM is the straightforward and easy implementation of the method. The disadvantage is that it is difficult to describe smooth surfaces such as the surface of the heart without steps, so that it becomes difficult to implement boundary conditions.

The FEM provides an alternative way of representing discrete space. Potentially complex cardiac tissue geometry is divided into small sub-domains, called "finite elements", which can be described and handled in a simplified manner. These finite elements can have non-uniform size and shape. Inside each element, the solution is approximated by an interpolation function. The FEM is widely used because of its well-developed theory allowing for variable mesh representations and interpolation of material properties. A particular advantage is that complex, curved geometries can be modelled accurately, see for example (Vigmond et al., 2002). The FEM method has been used by many groups in this research field, especially for simulations with anatomically detailed geometry. The disadvantage of the FEM is the higher effort compared to the FDM both for development and running the software.

For the FVM, volume integrals in a PDE involving a divergence component are converted to surface integrals applying the divergence theorem. This method is conservative because the flux entering a volume is identical to the one leaving the neighbouring volume. The FVM can be applied easily to unstructured meshes. It also has been used in bidomain modelling (Courdiere and Pierre, 2006; Harrild and Henriquez, 1997; Jacquemet and Henriquez, 2005; Trew et al., 2005a). Since the method is conservative, a coupling between excitation propagation in the heart and the electrical field in the body can be easily achieved (Courdiere and Pierre, 2006).

The FDM, FVM and FEM applied to Poisson's equations lead to large sparse, symmetric matrices. Methods for solving these are described in Section 6.4 onwards.

Simulations of action potential propagation require boundary conditions, including permanent conditions at tissue boundaries as described in equations (7) and (11) (usually Neumann or no-flux boundary conditions) and possibly time dependent boundary conditions, which can be current or voltage stimuli in the intra- and extracellular space at given points in time. Boundary conditions (Dirichlet boundary conditions) associated with setting potentials can be applied to the LSE after its generation by changing the respective entries or line and column in the matrix and the respective entry in the right hand side vector. With the bidomain model, a permanent zero potential is frequently set in the extracellular space at the boundary. For complex tissue geometries no-flux boundary conditions can be implemented using a phase-field approach (Fenton et al., 2005).

6.4. Implicit, explicit and semi-implicit solution schemes for discrete time

Explicit, implicit, and semi-implicit (also called IMEX) methods can be used to solve the equations describing the time dependence of action potential propagation. The choice of numerical method influences the stability, computational cost and the accuracy of the implemented model.

Explicit methods have been used extensively (Barr and Plonsey, 1984; Henriquez and Plonsey, 1990; Penland et al., 2002; Pollard and Barr, 1991; Roth, 2001; Vigmond et al., 2002), because they are easy to implement. However, even though the computational cost for each time step is low in an explicit method, the time step may need to be small to guarantee stability for the diffusion operator (Press et al., 1992); specifically, the condition $\Delta t \leq \Delta x^2/(2dD)$ must be satisfied, where d is the system dimension (1, 2, or 3), D is the diffusion coefficient, Δt is the time step, and Δx the space step. Implicit schemes can be stable with longer time steps (Bourgault et al., 2003; Hooke et al., 1994; Munteanu et al., 2009; Murillo and Cai, 2004), but require solution of a non-linear system of equations at each time step, and so are more computationally expensive. A good compromise between these two methods is a semi-implicit IMEX scheme, in which some terms of the equations (e.g., the linear terms) are solved implicitly and the remaining terms (e.g., the non-linear terms) are solved explicitly. The stability constraints of IMEX methods are less demanding than fully explicit methods but more than fully implicit methods. Since the linear terms are usually solved implicitly in an IMEX method, a solution of a linear system is required at each time step. The IMEX methods can be classified on the basis of the order of approximation they can achieve. First-order methods are the most common (Colli Franzone and Pavarino, 2004; Keener and Bogar, 1998), although higher order IMEX methods have been proposed. An extensive stability analysis of IMEX methods for solving the bidomain equations coupled with the FitzHugh-Nagumo kinetic model can be found in (Ethier and Bourgault, 2008), together with a comparison of computational costs.

6.5. Linear system solvers and preconditioners

Most numerical approaches to solve tissue electrophysiology models result in a linear system of equations. Linear solvers can be classified as direct solvers and iterative solvers (Demmel, 1997). The first group is composed of methods that compute the solution of the linear system by direct manipulation of the original matrix, like computing a factorisation or a Gaussian elimination. In theory, these methods can be efficient and produce exact solutions. However, rounding errors can become significant, and exact solutions are not obtained. In addition, these methods require large amounts of memory and CPU time for the initial decomposition, although the factorisation of the matrix needs to be computed only once if the matrix does not change during the time evolution. LU factorisation is one of the most common direct solvers, together with the Cholesky factorisation for symmetric matrices. Since one drawback of this kind of approach is that the pattern of the original sparse matrix can be filled during the process, a renumbering strategy can be employed.

The most widely used approach is iterative solving. Approximate solutions of the linear system are computed until a stopping criterion (usually an error tolerance) is reached. Most published approaches for discretisation of monodomain and bidomain models leads to symmetric matrices. In this case a common option is the Conjugate Gradient method (CG) or its variations like the BiConjugate Gradient Stabilized (BICGSTAB) method. However in some cases, due to the formulation chosen and numerical scheme implemented, non-symmetric matrices may arise (Gerardo-Giorda et al., 2009; Pennacchio and Simoncini, 2009) requiring an alternative method to solve the system. In these cases Krylov subspace solvers are extensively used, in particular the Generalised Minimal Residual Method (GMRES). We refer to (Saad, 2003) for details about the algorithms mentioned.

To speedup the convergence of iterative solvers, several types of preconditioners can be used to transform the initial linear system into an equivalent system whose associated matrix has better spectral properties such as a lower condition number or improved clustering of the Eigenvalues. One common option is to compute an incomplete LU (or an incomplete Cholesky) factorisation, preserving a pattern

similar to that of the original matrix, and to use this new matrix as a preconditioner for the system. This approach has been shown to be effective on serial architectures (Ethier and Bourgault, 2008). A comparison using a parallel architecture has shown that a CG solver preconditioned by a domain decomposition parallelisation of an incomplete LU factorisation to be twice as fast as the same solver preconditioned with a Jacobi preconditioner (Potse et al., 2006). In another study (Colli Franzone et al., 1998) a CG solver preconditioned by Symmetric Successive Over-Relaxation preconditioner was used for solving the eikonal model. In (Gerardo-Giorda et al., 2009) the authors propose a specific preconditioner for the bidomain problem consisting of a model-based block triangular preconditioner obtained after a proper reformulation of the monodomain model. This approach reduced the CPU time required by the incomplete LU preconditioned CG solver on serial architectures by 50%.

Multigrid methods have been employed for the solution of mono- and bidomain models. Multigrid methods are based on the combination of an iterative solver running on fine computational grids of the domain and a direct solver running on a coarse grid of the same domain (Hackbusch, 1985). The rationale behind these methods is that, while the high frequency component of the error in the solution can be reduced quickly using an iterative solver on a fine grid, the low frequency (smooth) component of the error can be reduced efficiently by using a direct solver on a coarse grid.. By repeating these steps both the high and the low frequencies of the residual of the linear system can be reduced efficiently within a specified tolerance. Multigrid methods have been employed as solvers in sequential implementation (Keener and Bogar, 1998). They have been also used as preconditioners for other solvers (such as CG) both in sequential (Sundnes et al., 2002) and in parallel implementations (Weber dos Santos et al., 2004a). Multigrid methods can also be adapted for local changes in conductivity for modelling discontinuous tissue (Austin et al., 2006). Studies that compared multigrid preconditioners with standard incomplete LU preconditioned CG in sequential and parallel implementations, demonstrated higher efficiency of multigrid preconditioners (Plank et al., 2007; Weber dos Santos et al., 2004b). In parallel implementations the optimal number of levels of the multigrid approach depends on the number of processors and on the available memory (Vigmond et al., 2008).

In (Pavarino and Scacchi, 2008) the authors propose and analyze a Multilevel Additive Schwarz preconditioner for the bidomain system. This approach overcomes the multiplicative nature of multigrid methods, which limit the extent to which they will scale in parallel implementations. This type of preconditioner has been shown to be both scalable and to offer a potentially optimal approach on structured meshes (Munteanu et al., 2009).

6.6. Temporal and spatial resolution

Choosing an appropriate spatial and temporal resolution for a tissue model is a complex decision that depends on the numerical method, cell electrophysiology model, diffusion coefficients and their anisotropy ratio, and geometrical properties of the tissue anatomy. It is important not only to guarantee numerical stability, but also to ensure that the solution fulfils requirements regarding accuracy. The underlying motivation is to ensure that rapid processes, such as the action potential upstroke, are sufficiently resolved in time and, similarly, that sharp spatial gradients, such as a propagating wavefront, are sufficiently resolved in space. The optimal way to consider these requirements is to choose the resolution based on the features of the reaction–diffusion properties. The upstroke velocity of the action potential determines the upper limit of the time step, and the size of the wavefront the space step. However, there is little consensus about what these values ought to be. Simulations of larger tissue volumes typically employ a spatial resolution of between 0.1 and 0.2 mm, with a time step of between 0.01 and 0.02 ms for the diffusion component of the model, with a smaller time step for the cell membrane kinetics. A pragmatic approach is to compare the conduction velocity found using given spatial and temporal resolutions with a solution obtained using smaller or larger resolutions and to consider the resolution adequate when these solutions converge. However, this approach may not always be practical, especially for 3-D simulations, where using a spatial resolution twice as fine increases the computational cost by a factor of eight. In addition, altering the spatial resolution requires remeshing, which can be a complicated and time-consuming procedure when non-uniform grids are used. Some mesh generation software may be unable to produce finer meshes because of restrictions on the number of elements.

In practice, a common procedure for ensuring converged results is to measure CV for different resolutions and to consider the resolutions used adequate when finer resolutions give close results (often, within five or ten percent). CV is quite sensitive to spatial resolution, much more so than other quantities like APD. Fig. 11 shows examples of CV and APD as a function of spatial resolution for two models solved using an explicit Euler method with the FDM. In this case APD was insensitive to resolution for the values used. In contrast, CV was sensitive. The temporal resolution is also important; however, for the range of spatial resolutions considered here the time step was constrained by the stability criterion for the explicit Euler method, and hence little error was incurred by the time step selection. When using implicit or semi-implicit methods, larger time steps can be used without incurring instability in the numerical method, but a time step that is too large, like a space step that is too large, can yield unacceptable errors in CV, as has been shown previously (Cherry et al., 2003; Courtemanche, 1996).

In two or more dimensions, spatial resolution can play a significant role in determining the system dynamics. With insufficient resolution, curved wave-fronts can develop corners; with standard FDMs on uniform Cartesian grids, these corners tend to develop in the fronts at 45-degree angles from the coordinate axes. Fig. 12 shows rotating spiral waves for the Nygren et al. model (Nygren et al., 1998) obtained at different spatial resolutions with the same temporal resolution. The spirals obtained using coarser resolutions show clear signs of under-resolution. The resolution required to avoid these distortions varies from model to model and depends largely on the steepness of the upstroke. For example, 0.25 mm is an adequate resolution for the Nygren et al. model, as shown in Fig. 15, but for the Fox et al. model, which has a faster upstroke, a finer resolution of 0.15 mm is required.

In addition to overt signs like wave-front distortions, spatial resolution also can affect other properties of spiral waves. Fig. 12 also shows the spiral wave tip trajectories obtained for different spatial resolutions during the last 5 s of a 60 s simulation. When coarser resolutions are used, the trajectory obtained increases in size; the wavelength decreases as well. In addition, although the tip trajectory differences are relatively small, the spiral period depends more strongly on resolution. Here spiral periods of 352, 352, 358, and 391 ms are obtained for resolutions of 0.125, 0.25, 0.5, and 1 mm, respectively. The coarsest resolution, then, gives a spiral period 11% longer than the finest resolution. This type of change in period can produce significant differences in dynamics for more complex spiral wave trajectories and consequently result in erroneous stability or instability.

When anisotropy is introduced, additional resolution constraints apply. The safest choice is to use a resolution sufficient for the smallest diffusion coefficient (or conductivity) of the system. It may be possible to use a resolution between what is sufficient for

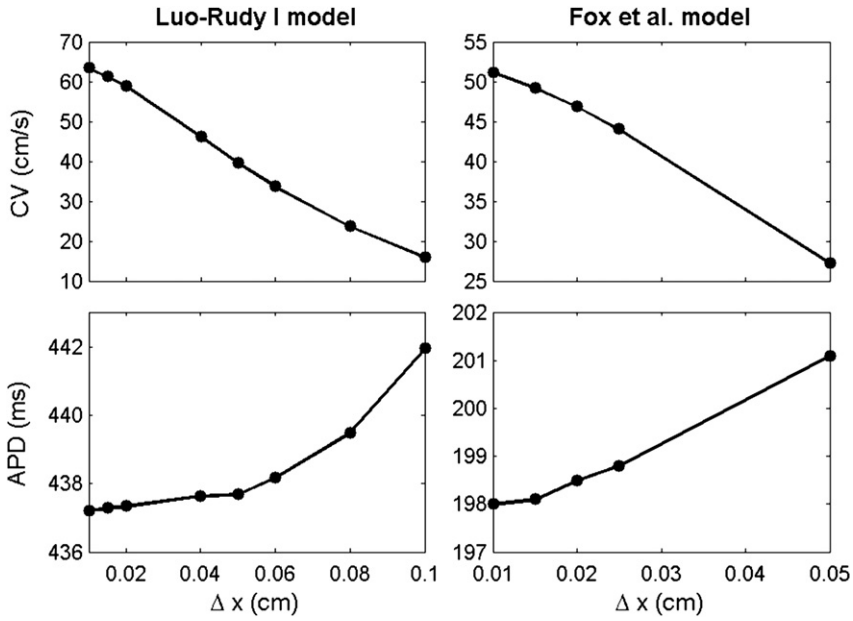

Fig. 11. Dependence of conduction velocity (CV) and action potential duration (APD) on spatial resolution for the Luo-Rudy 1 and Fox et al. models using an explicit Euler integration method. CV in general is much more sensitive to resolution than APD. Although a fixed temporal resolution of 0.005 ms is used here, using an implicit or semi-implicit method to take time steps above the explicit Euler stability limit can produce large errors in CV as has been shown previously (Courtemanche, 1996; Cherry et al., 2003).

the smallest and largest diffusion coefficients, but this has not been demonstrated. One way to quantify whether the spatial resolution is adequate is to examine the shapes of elliptical waves initiated in 2-D domains with a fixed anisotropy ratio but varying fibre angles. Fig. 13 shows an example of how such data can be used. Fixed voltage contours are obtained for multiple fibre angles using a given spatial resolution, and are then rotated back to align with the *x*-axis. The eccentricity of the rotated ellipse is then calculated for each fibre angle. For inadequate resolution, the eccentricity depends strongly on the fibre angle. As the spatial resolution becomes finer, the dependence decreases, but in general rather fine spatial resolution is required to eliminate the dependence. The eccentricity values are model-dependent as well, with models characterised by slower upstrokes requiring a coarser resolution than those with faster upstrokes.

In addition to these issues of conduction velocity, wave-front shape, spiral trajectory, and rotation period, inadequate spatial resolution has been shown to affect dynamics in other ways. Coarse resolution can induce spiral wave breakup when finer resolution results in stable spirals (Fenton et al., 2002; Panfilov and Keener, 1995). The opposite also can occur, with coarse resolution (or fewer connections between grid points) producing stable trajectories, but finer resolution resulting in breakup (Bueno-Orovio et al., 2008; Panfilov, 2002). For media with low excitability, spiral waves can even pin to the lattice and follow (for a uniform grid) quasi-rectangular trajectories (Fenton et al., 2002). Overall,

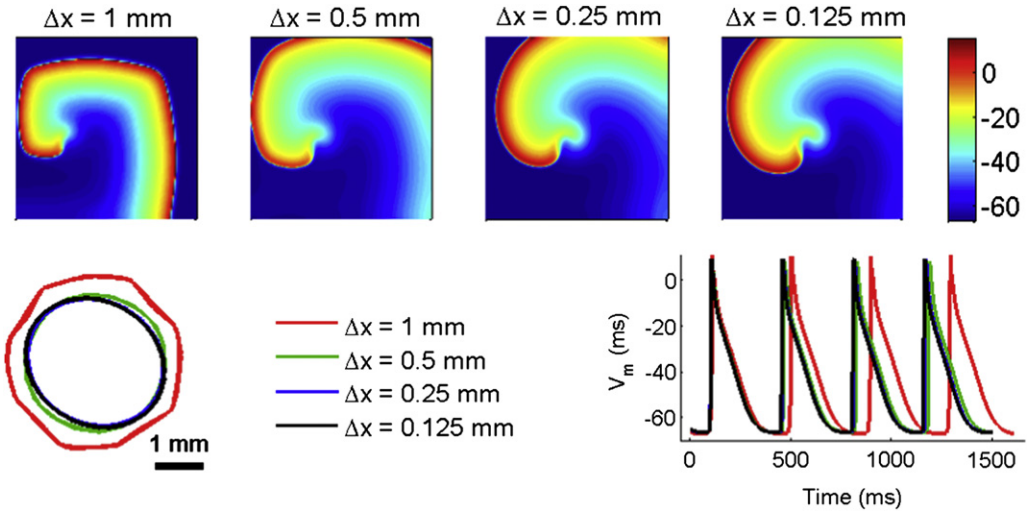

Fig. 12. Spiral waves and tip trajectories obtained after 60 s of simulation time using the Nygren et al. model in a two-dimensional sheet (10 cm × 10 cm) as a function of spatial resolution. Although the solutions for 0.25 and 0.125 mm agree well, indicating adequate resolution at 0.25 mm, the solution is under-resolved for coarser resolution. The presence of "corners" at 45° from the coordinate axes indicative is a sign of inadequate resolution and can be seen for the solution using 0.5 mm, although it is much more pronounced when the spatial resolution is 1 mm. The spiral tip trajectories also vary, with the coarsest resolution demonstrating significant lattice pinning by the presence of corners within the trajectory. Different periods are also produced, with coarser resolutions displaying longer periods.

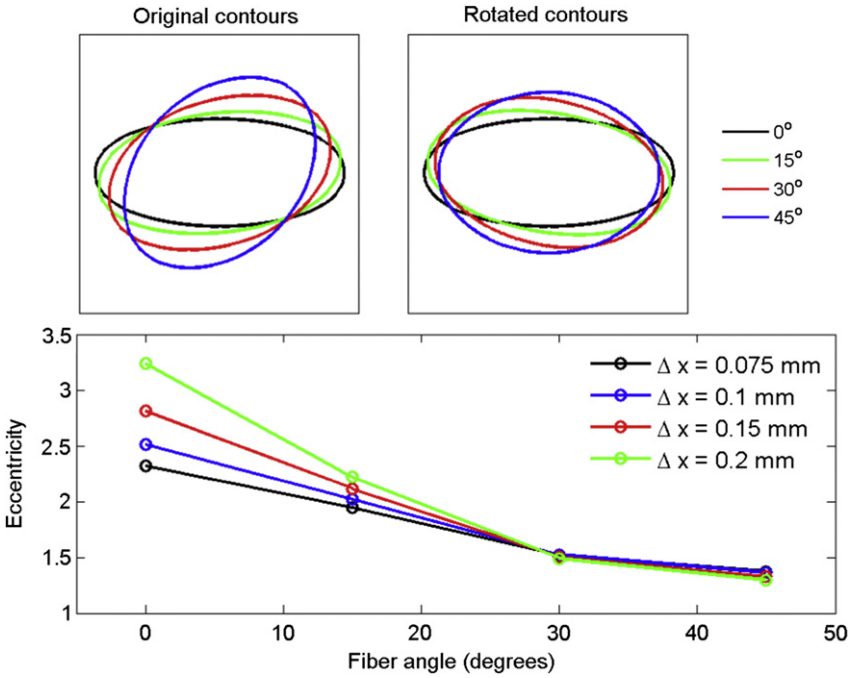

Fig. 13. Eccentricity of ellipsoids formed from a centrally located point stimulus as a function of uniform spatial resolution and constant fibre angle for the Fox et al. model in a two-dimensional sheet (3 cm × 3 cm). Anisotropy ratio is 5:1 (corresponding to diffusion coefficients of 0.001 and 0.0002 $cm^2\ ms^{-1}$ along and across fibers, respectively). Top: contours at −30 mV after 20 ms of propagation for a spatial resolution of 0.075 mm. Rotated contours are obtained by rotating the ellipses by the fibre angle to align with the *x*-axis. Bottom: Eccentricity is calculated for the rotated contours by taking the ratio of the width to the height. For the range of spatial resolutions used, the shape of the ellipsoids depends strongly on the fibre angle, with a maximum eccentricity for fibers aligned to the coordinate axes. The dependence decreases as spatial resolution increases.

although it is known that variations in spatial resolution can result not only in quantitative but also in qualitative dynamical differences, there is at present no method to guarantee adequate resolution in the absence of such a comparison beyond reporting that a given solution agrees well with a solution obtained using finer spatial and temporal resolution.

6.7. Parallel implementation

Various parallel implementations of solvers have been developed and applied for simulations of tissue electrophysiology. For example, some simulators (Potse et al., 2006) are based on on OpenMP (Open Multi-Processing, http://openmp.org/), an implementation of multithreading that supports shared memory architectures. The main advantage of OpenMP is that implementations can be easily adapted for parallel execution, since the serial implementation needs only to be slightly modified or can use OpenMP indirectly by interfacing with specific linear algebra packages able to deal with OpenMP. An alternative approach is based on MPI (Message Passing Interface, http://www.mpi-forum.org/), a message-passing application programming interface that allows codes running on many computers to communicate with one another. In this case, specific code has to be developed to deal with MPI, but high scalability can be achieved. MPI based code can run on both distributed and shared memory architectures. The principal advantage of MPI is that it allows usage of systems with distributed memory architectures, which have only a fraction of the cost of systems with shared memory. Examples of this programming strategy applied to tissue electrophysiology simulations can be found in (Colli Franzone and Pavarino, 2004; Pavarino and Scacchi, 2008). An intermediate approach involves developing hybrid code that can take advantage of computer architectures, which are a hybrid combination of shared and distributed memory (Bordas et al., 2009).

7. Strategies for reducing calculation time

A number of pragmatic approaches apart from standard numerical methods can be used to reduce the time required to run simulations of cardiac tissue electrophysiology. In the following section we describe some of the most effective and well established techniques, as well as some more novel approaches.

7.1. Lookup tables

Many models of cellular electrophysiology require computationally expensive functions, such as exponentials, logarithms, trigonometric functions, and exponentiation to be evaluated. These functions often depend purely on V_m, and significant computational speedup can be obtained by pre-computing these values and storing them in lookup tables that are used for subsequent evaluation (Victorri et al., 1985). The tables can be arranged as 1-D arrays corresponding to a physiological range of voltages with a fine enough resolution to capture differences (generally on the order of 0.01–0.1 mV) (Cherry et al., 2003). Often, combinations of these expensive functions can be evaluated and stored together so as to minimize their calculation within the time-stepping process. Although choosing the nearest voltage value represented in the table is one possibility, linear interpolation can be used to interpolate between the two nearest voltage values represented in the table for increased precision. Speedup achieved depends on the number and type of functions replaced by lookup tables: the more computationally expensive the function, the greater the resulting speedup. Exponentiation to non-integer powers are often the most expensive, followed by exponentials and trigonometric functions, although system architecture, compiler choice, and function argument ranges affect the relative cost of evaluating such functions. Nevertheless, it is possible to achieve a speedup factor of up to 5 (Cherry et al., 2003).

Lookup tables can also be used for computationally expensive functions that are dependent on other variables, such as intracellular calcium concentrations and even some transmembrane currents. It is also possible to construct a 2D table for computationally expensive functions that depend on two state variables. An example can be found in the Hund-Rudy model (Hund and Rudy, 2004), where the *d*-gate is raised to a variable power. Because exponentiation is usually such a costly function to evaluate, and because the two quantities involved have limited ranges (the *d*-gate varies strictly between 0 and 1, while the variable power takes values between 1 and 9), use of a 2D lookup table can save computational time with little effort.

It is important to note that lookup tables may not be suitable for representing certain quantities that exhibit large changes for small changes of function variables. If the table size needed to represent such quantities is extremely large pre-calculation may be time-consuming, and memory requirements or memory access times may become prohibitive. An alternative is to use lookup table values within certain values and to calculate the quantity directly otherwise, which can be accomplished with a simple *if*- statement in the code. Careful coding of the model equations can further add to the benefits of lookup tables. This can be done using automated tools, and can result in substantial speedup (Cooper et al., 2006). In all cases, the application of lookup tables for a given model within a particular code should be evaluated to ensure acceptable accuracy is maintained.

7.2. Exponential solutions for gating variables

For explicit time-stepping schemes, speedups can be obtained in many cases by integrating the gating variables for the cell model ODEs using exponential solutions (Maclachlan et al., 2007; Plank et al., 2008; Rush and Larsen, 1978). This method applies to an individual gating variable y represented by the ordinary differential equation.

$$\frac{dy}{dt} = (y_\infty - y)/\tau_y. \tag{18}$$

With a steady-state value y_∞ and the time constant τ_y. If voltage is considered to be non-varying over a single time step, this can be solved analytically over that time step as

$$y_{n+1} = (y_\infty - y_n)\exp(-\Delta t/\tau_y), \tag{19}$$

where y_∞ and τ_y are solved using V_n, the value of the membrane potential at the old time step, and Δt is the time step. Similar benefits can also be achieved by integrating using a semi-implicit integration scheme under the same assumption that y_∞ and τ_y are constant over the time step (Cherry et al., 2003; Whiteley, 2006).

The primary advantage of this method is to allow a larger time step than a purely explicit integration scheme while retaining accuracy. The value of the exponential can be pre-computed and stored in a lookup table to avoid computationally expensive function evaluations. However, the technique solves the set of ODEs in a decoupled form, which makes the solution first-order-accurate, although it is possible to extend the approach to achieve second-order accuracy (Sundnes et al., 2009). In addition, calculation of other variables, such as ionic concentrations, cannot benefit from this approach.

7.3. Operator splitting

The global system of PDEs and ODEs can be decoupled in several ways by operator splitting, with the aim of improving the computational efficiency and reduce complex dependencies between the variables of the problem. In principle, these methods introduce a splitting error that is independent of the numerical methods used to solve the decoupled components. This additional error should be quantified, unless the split steps are re-iterated until a suitable convergence condition is satisfied. In general, splitting techniques that alternate between two decoupled operators are first-order-accurate. However, second-order accuracy can be achieved by performing two half-steps with one operator before and after a full step of the second operator (Strang, 1968).

In (Roth, 1991; Roth and Wikswo, 1994) an operator splitting technique on a finite-difference formulation is used to solve the bidomain problem coupled with a PDE representing the surrounding bath. In (Qu and Garfinkel, 1999) a second-order-accurate splitting technique has been proposed to separate the solution of the monodomain PDE describing propagation in tissue from the Luo-Rudy phase I ODEs describing local membrane kinetics. However, the ODE system was solved using the Rush-Larsen method (Rush and Larsen, 1978), while the time advancing scheme for the PDE was an explicit forward Euler method, which resulted in the algorithm being only first-order-accurate overall. An operator splitting technique has also been devised for solving the bidomain equations coupled with a description of volume conduction in the torso (Sundnes et al., 2005). In this study the authors proposed a general formulation of operator splitting, based on a θ-rule, that can result in a second-order scheme for a proper choice of the parameter. The ODE system was solved using a third order Runge-Kutta scheme. The ODE system itself can be decomposed using operator splitting methods. Operator splitting techniques applied to the bidomain equations are reviewed in (Vigmond et al., 2008), where a three-step operator splitting for decoupling the bidomain system that has been proven to be unconditionally stable is described.

7.4. Efficiency of adaptivity in space and time

A major challenge for increasing numerical efficiency is the use of adaptivity in space and time. Although there is a rich numerical literature on adaptivity for both finite-difference and finite-element methods, dynamic and simultaneous adaptivity in space and time in which both the spatial and temporal resolution are varied locally over the course of the simulation has only rarely been applied to cardiac electrophysiology studies (Cherry et al., 2000, 2003; Colli Franzone et al., 2006; Deuflhard et al., 2009; Trangenstein and Kim, 2004). In contrast, dynamic temporal adaptivity has been used more commonly (Allexandre and Otani, 2002; Qu and Garfinkel, 1999; Quan et al., 1998; Vigmond and Leon, 1999) and dynamic spatial adaptivity also has been used (Belhamadia et al., 2009; Pennacchio, 2004). The general idea behind dynamic space-time adaptivity is that the algorithm can increase or decrease spatial and temporal resolution locally during times when such adjustments are beneficial (e.g., higher resolution for action potential upstrokes and associated sharp spatial gradients and lower resolution during quiescence). Developing dynamically adaptive methods is a complex endeavour. Also, characterising accuracy and efficiency of such techniques is not straightforward. One significant challenge in measuring the speedup provided by adaptive methods is that their efficiency generally depends on the dynamical state simulated, including the wavelength, wave-front width, and density of waves in the domain. For simple plane wave propagation with long periods during which no wave is present in most of the domain, adaptive methods can provide a speedup of more than an order of magnitude. The efficiency gains in the presence of more complex spatiotemporal dynamics are generally more modest but still can be significant. A space–time–adaptive finite-difference approach was found to give a speedup of a factor of 20 for a plane wave in a 2-D domain (Cherry et al., 2000) and 50 for a plane wave

in a 3-D slab with rotational anisotropy (Cherry et al., 2003), but still managed a factor of five for a 2-D domain with sustained spiral wave breakup (Cherry et al., 2000), in all cases compared to a uniform mesh using the finest spatial and temporal resolutions available to the adaptive algorithm.

A different space–time–adaptive method using finite elements gave a speedup factor of less than a of two in a two-dimensional domain during initiation and about one rotation of a spiral wave (Trangenstein and Kim, 2004). Another approach using an adaptive multilevel FEM with a linearly implicit Rosenbrock discretisation with stepsize control in time achieved a reduction of two orders of magnitude for both the number of computational nodes and the number of time steps taken for a single propagating plane wave in a 3-D domain using the bidomain equations (no measure of speedup was given) (Colli Franzone et al., 2006). This approach recently was extended to realistic cardiac geometries (Deuflhard et al., 2009). Similar work is underway to extend the work of Cherry et al. (Cherry et al., 2003) to realistic anatomies by combining it with the phase-field approach (Fenton et al., 2005), as shown in Fig. 14. In addition to a dependence on the dynamical state, the speedup achieved also depends on the electrophysiology model: because the computational costs associated with regridding and other numerical tasks are fixed, computationally more expensive models can benefit more from adaptivity than simpler models.

A related approach is to use increased spatial resolution only for the variables associated with the rapidly varying I_{Na}. This technique has been shown to increase computational efficiency for plane wave simulations using the bidomain model with the Noble et al. guinea-pig ventricular model (Noble et al., 1998) by two orders of magnitude (Whiteley, 2008); however, it is unclear whether similar performance gains would be achieved for larger domains with more complex dynamical states containing multiple interacting waves.

7.5. Using graphics processing units for computation

The increased computational power and memory of graphics processing units (GPUs), combined with decreasing costs, has generated significant interest in utilising graphics hardware for other applications. GPUs have been optimised for traditional computer graphics, which is focused on highly data-parallel operations on floating-point numbers, and provide less of an advantage for activities outside this range, such as intensive memory communication and integer and double precision calculations (Owens et al., 2007). Nevertheless, many computationally demanding calculations may benefit from GPUs, which have already been applied to simulations outside graphics and visualisation applications, including cellular automata, dendritic growth, fluid and gas dynamics, signal and image processing, geometric computing, and reaction–diffusion equations (Owens et al., 2007). Recent work demonstrated significant speedup of simulations of cardiac electrophysiology equations in tissue (Sato et al., 2009; Vigmond et al., 2009). However, it remains to be seen how effectively GPUs can be integrated into large-scale cardiac simulations.

7.6. Use of simplified cell models for representing tissue

Large-scale tissue simulations may involve millions of grid points. To improve computational tractability in these cases, simplified cell models represent an alternative to more biophysically detailed models. Whereas detailed cell models may include 30–100 variables and tens to hundreds of equations, simplified models generally include between two and ten variables and a correspondingly reduced number of equations. Such a reduction in the computational workload can translate into a speedup of one or more orders of magnitude, although this depends on how the diffusion calculation is implemented (see Section 6). In some cases, reduced models also have less restrictive spatial and temporal resolution requirements and can achieve further computational savings by using coarser resolutions.

Simplified models used for cardiac electrophysiology tissue simulations generally fall into three categories: direct reductions of more detailed models, generic models, and phenomenological models. Below we discuss each of these types of simplifications, including the advantages and limitations of each approach.

7.6.1. Reductions of detailed models

Reduced models are developed by reducing the complexity of a detailed model through any of several means. Rapidly varying variables, such as the *m*-gate governing activation of I_{Na}, may be eliminated adiabatically by using the steady-state value, thereby assuming that the gate instantaneously achieves the steady-state value associated with a given voltage. This approach not only eliminates a variable but also eliminates a significant source of stiffness in the differential equations, so that larger time steps can be used in the numerical scheme. However, unacceptably large errors can result. For example, eliminating the *m*-gate adiabatically in a reduction of the Priebe-Beuckelmann model results in significantly decreased conduction velocity (Bernus et al., 2002). Additional gating variables also can be eliminated either by removing slowly varying gates or by combining variables, such as the two voltage-dependent inactivation gates used in many representations of I_{Na} (Bernus et al., 2002). Another common approach to reduce the number of variables is to treat many or all intracellular ion concentrations as constant. Although this can produce computationally desirable benefits, such as decreased accommodation time after a change in the pacing cycle length, treating concentrations as

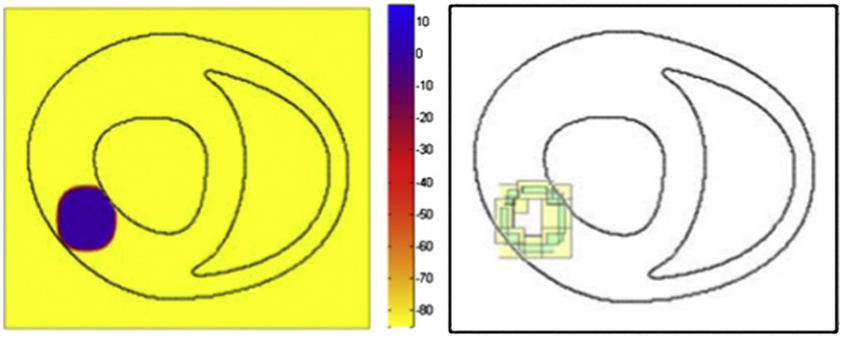

Fig. 14. Adaptive mesh refinement in a 2-D slice of canine ventricles from (Nielsen et al., 1991). Left: Voltage plot 160 ms after a stimulus applied in the lower left using the Luo-Rudy phase I model (Luo and Rudy, 1991). Right: Three-level grid structure corresponding to the voltage plot. Coarse mesh regions (0.5 mm) are shown in white, fine (0.125 mm) in green, and intermediate (0.25 mm) in yellow.

constants can remove other important properties, such as memory. Finally, currents with small values, such as background currents or the sarcolemmal Ca^{2+} pump, in some cases may be eliminated (Mahajan et al., 2008). For models involving detailed Markov representations of currents, reductions can be accomplished by substitution with less complex Hodgkin-Huxley-style descriptions, by using rapid equilibrium assumptions, or by replacing ODEs with algebraic equations when transients are fast enough to be considered instantaneous (Henry and Rappel, 2004; Hinch, 2004; Plank et al., 2008).

The main advantage of reduced models is that they improve computational tractability while retaining a similar structure as the more detailed model. In this way, it is easier to incorporate biophysical variations, such as spatial gradients in channel expression, the effects of pharmaceutical agents, and electrophysiological remodeling effects. However, the reduction may reduce or eliminate important properties of real cells and tissue such as memory. Furthermore, the reduction process must be undertaken separately for each detailed model to ensure that the desired properties are preserved with each variable eliminated.

7.6.2. Generic models

Generic excitable media models, such as the FitzHugh-Nagumo (FHN) model (Fitzhugh, 1961), have been used to illustrate properties of wave propagation for many years. The FHN model itself is a 2-variable reduction of the Hodgkin-Huxley model (Hodgkin and Huxley, 1952) and in its original form produces action potentials more like neural action potentials. The FHN model can be modified to produce longer action potentials and to eliminate hyperpolarisation that occurs during the depolarisation phase. However, the FHN model and others like it generally lack other important properties, including realistic APD restitution, memory, and a non-zero minimum cycle length (and corresponding APD) below which block occurs. Without these more realistic properties, generic models often are of limited use and are generally restricted to showing the types of qualitative behaviour that may occur with more detailed models. As computational resources have increased, generic models have been used less often. Nevertheless, one of the main advantages of generic models remains, which is the relative ease with which analytical results can be obtained.

7.6.3. Phenomenological models

A third approach to reducing computational complexity is to develop phenomenological models that aim to reproduce key dynamical properties of cells and tissue without including as much biophysical detail. For example, rather than including the descriptions of ten or more ion channels, pumps, and exchangers, a phenomenological model may focus on "summary" inward and outward currents that rely on fewer variables and equations. The Fenton-Karma model (Fenton and Karma, 1998) and its subsequent extensions (Bueno-Orovio et al., 2008; Cherry and Fenton, 2004) are examples of phenomenological models. Originally, it included 3 variables and 12 parameters together with three currents, representing the fast inward, slow inward, and slow outward currents. Extended versions of the model have increased the number of variables to 4 and the number of parameters to 28 (Bueno-Orovio et al., 2008); these additions allow spike-and-dome action potential shapes to be reproduced. Among the dynamical properties that are incorporated are the threshold of excitation, maximum upstroke velocity, action potential shape, APD, APD and CV restitution curves, and the minimum cycle length (greater than zero) below which propagation fails.

Because these models focus on reproducing dynamical properties rather than detailed ion currents, they can be fit directly from tissue-level experimental data that measure these quantities, rather than from patch-clamp data obtained from isolated cells. The small number of variables and parameters makes parameter fitting much more straightforward, as many parameters govern or contribute to only a single property. In addition to fitting experimental data, the model can be used to fit data from more biophysically detailed models (Bueno-Orovio et al., 2008). For example, as shown in Fig. 15,

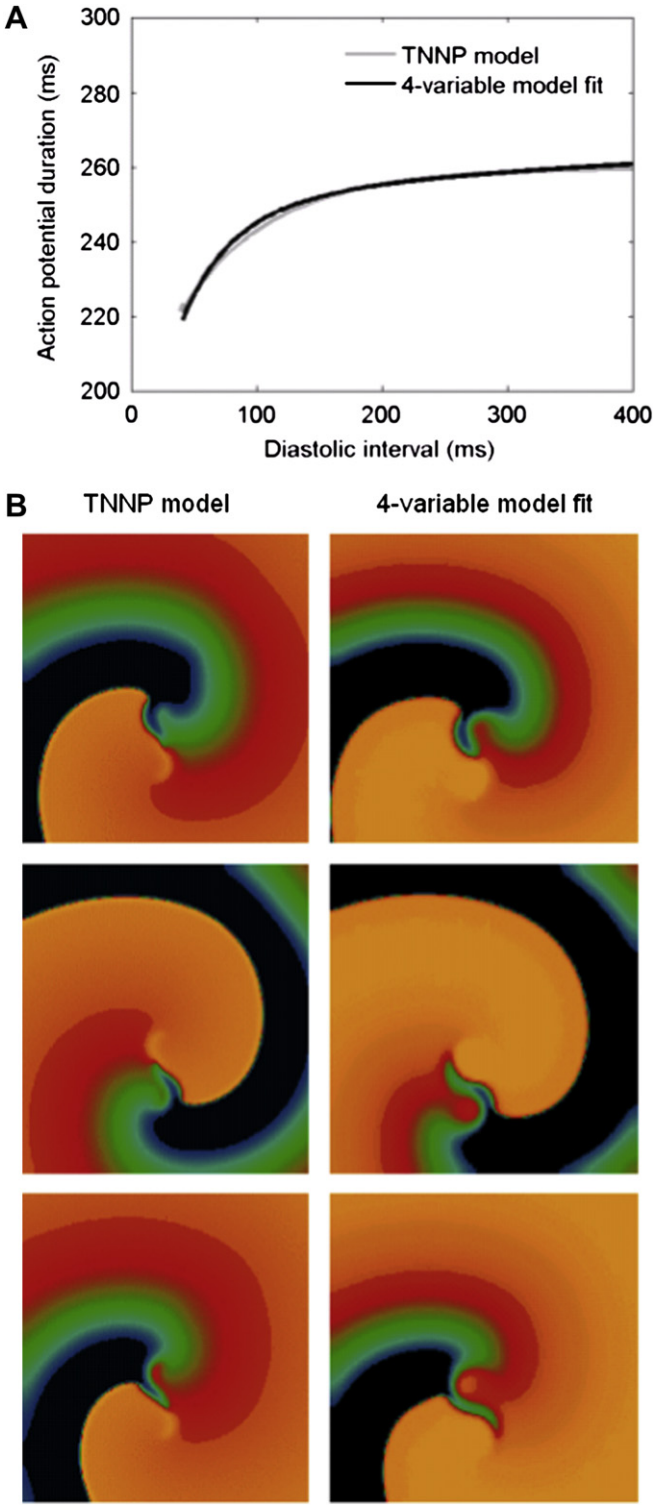

Fig. 15. Original TNNP and the 4-variable model fit to it (see text for details). A. Restitution curves for the TNNP model (grey) and the 4-variable fit. B. Spiral wave at three times during a single rotation for the TNNP model (left) and the 4-variable fit (right).

the model can successfully reproduce the restitution curve and spiral wave dynamics of the ten Tusscher et al. model for human ventricular cells (TenTusscher et al., 2004). The Priebe-Beuckelmann model (Priebe and Beuckelmann, 1998) also has been fit (Bueno-Orovio et al., 2008).

In addition to improving computational tractability, one of the advantages of phenomenological models is the relative ease with which specific dynamical properties can be implemented. As an example, this model has been used to examine the effects of different action potential shapes on tissue dynamics (Cherry and Fenton, 2004). In this application, two different parameter sets were developed to produce action potentials with different shapes but with identical restitution and bifurcation properties in isolated cells for APD measured to 80 percent (or more) of repolarisation (see Fig. 16A and Fig. 16B). In tissue, both models also produce alternans, but CV restitution curves with more gradual slopes over a wider range of cycle lengths are able to reduce or even eliminate alternans for the model that repolarises more quickly. This can prevent spiral wave breakup that occurs for the other model, as shown in Fig. 16C.

A disadvantage of this approach is that reproducing the effects of ion channel blockers and other modifications of specific electrophysiological changes is not as straightforward. However, it is possible to perform a new parameter fitting to data obtained in the presence of the channel blocker, an approach that may be useful for novel pharmaceutical agents whose effects are incompletely characterised.

7.7. *Choosing an appropriate cellular electrophysiology model*

Most recent models of cardiac cellular electrophysiology have been designed to represent cells from specific regions (e.g., atria, ventricles, Purkinje) and in some cases sub-regions (e.g., ventricular epicardial, endocardial, midmyocardial) of the heart, as well as particular animal species (e.g., mouse, rat, guinea pig, rabbit, canine, and human). The number of models described in the literature has increased significantly in the recent past. However, a model for a specific combination of species and region may still not be available. Also, more than one model representing the particular combination of species and heart region of interest may be available, and in some cases only a small subset of models reproduce the properties of interest for a given study. For instance, alternans at fast pacing rates is a common phenomenon across a number of species, but not all models of such species show alternans. The Fox et al. canine ventricular model (Fox et al., 2002) has alternans, but the earlier Winslow et al. canine ventricular model (Winslow et al., 1999) on which it is based does not. Among rabbit ventricular models, the Mahajan et al. model (Mahajan et al., 2008) has alternans, but the earlier Shannon et al. model (Shannon et al., 2004), from which it derives most of its current formulations, does not. Thus, not all models are appropriate for investigating specific phenomena, and in some cases there may be no model that displays behaviours observed experimentally.

Furthermore, most cellular level models are validated for specific conditions, including temperature, pacing rate, ionic concentrations, sex, and age. The model may not be applicable outside these conditions. Most models are constructed using isolated cell data only and so may not be able to reconstruct the properties and behaviour of cells in tissue. It is also important to note that modifying a model by changing parameter values or equations may compromise the original validation.

Simplified models can be appropriate in many cases, especially for tissue studies. In many cases tissue phenomena such as spiral wave breakup are model-independent and can be obtained using any model with similar characteristics. In addition, simplified models avoid problems associated with large numbers of parameters whose values may not be known with great precision and with large number of variables whose individual effects cannot easily be discerned. Ideally, models should be as simple as needed to explain the phenomena of interest—but no simpler.

8. Discussion

Integrated models of cardiac tissue electrophysiology are being used in basic science investigations including studies of defibrillation

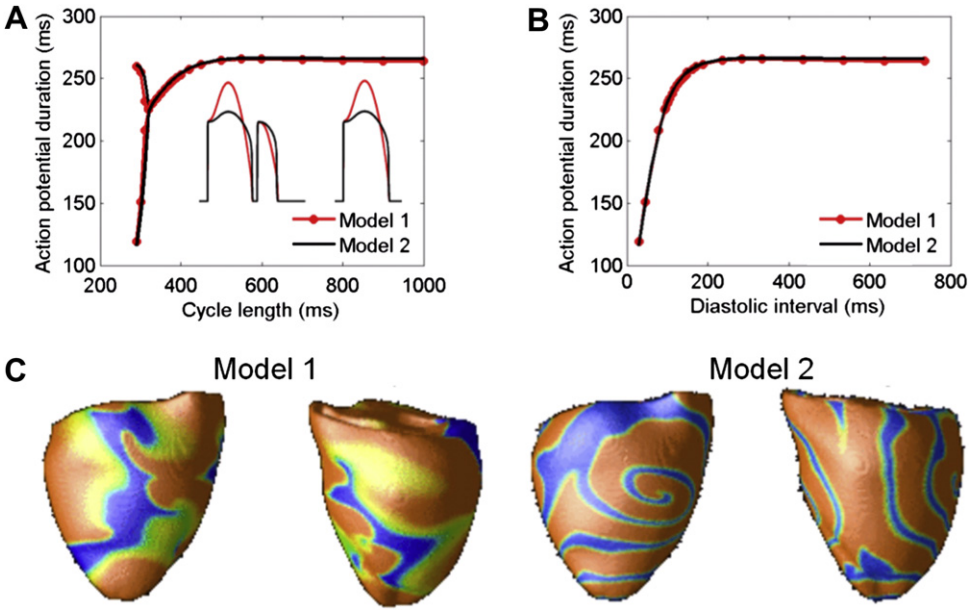

Fig. 16. Electrotonic effects on alternans and spiral wave stability. A. Bifurcation diagram showing APD as a function of cycle length in an isolated cell for two parameter sets (Cherry and Fenton, 2004). APD values below 80 percent of repolarisation match almost exactly, as shown for the inset action potentials at cycle lengths of 290 ms (during alternans) and 500 ms. B. Matching restitution functions for the same two parameter sets in isolated cells. C. Two views of spiral wave dynamics for the two parameter sets within a rabbit ventricular anatomy (Vetter and McCulloch, 1998). Although the APD restitution curves for the two models are identical in isolated cells, CV restitution in tissue modulates the effects of the steep APD restitution curve slope in tissue for Model 2 and produces a stable spiral wave.

(Rodriguez et al., 2005) and specific arrhythmias such as ventricular fibrillation (Ten Tusscher et al., 2009). Recently, highly detailed anatomical (Li et al., 2008; Plank et al., 2009) and patient specific models (Pop et al., 2009) have been introduced. Despite this progress, and increasing acceptance of models as research tools, there are few examples where models of cardiac electrophysiology have been useful in clinical applications. The reality falls short of the vision of the Cardiac Physiome Project, and there are some important issues that are not fully resolved; we have highlighted some of these in this review, and we continue this discussion below. From a philosophical point of view it is important to recognise that the purpose of modelling cardiac tissue electrophysiology is not only to reconstruct observed phenomena at ever greater levels of detail, but also to explain the mechanisms that underlie them and hence to predict the effects of changing parameters and other components of the model. All models involve assumptions and simplifications, and the tissue models reviewed here are simplifications of real cardiac tissue, its micro-structure and electrophysiological properties. For a particular model to be useful, it must capture enough detail at a particular level of complexity to offer a mechanistic insight that complements experimental work.

The heart is a complex multi-scale and multiphysics system, where cellular electrophysiology is coupled to metabolism and tension development, as well as to tissue mechanics and fluid dynamics. Fully coupled and integrative models of the heart are part of the vision for the cardiac Physiome, and although progress in this area is being made (Jie et al., 2010; Nickerson et al., 2006; Niederer and Smith, 2007; Panfilov et al., 2007), these large-scale models remain a significant future challenge. Within the narrower scope of tissue electrophysiological models, there are a number of challenges and open questions; we summarise and discuss some of these below.

8.1. Challenges

The increasing availability of high performance computing resources has a huge impact on computational research, in particular enabling simulations with more biophysical detail and higher throughput. These technological advances are driving the efforts in cardiac computational research towards more detailed and integrated models, with the goal of patient specific electrophysiological simulations that can be used clinically (Neal and Kerckhoffs, 2010; Plank et al., 2009; Pop et al., 2009). Balancing the amount of anatomical and biophysical detail against the time and data capacity required to perform simulations is an important issue. Underlying these considerations is the validity of the assumptions that are embedded in tissue electrophysiology models.

Understanding the functional relationship between the discrete structure and continuum behaviour of cardiac tissue at microscopic and macroscopic levels is a significant challenge. As described earlier in Section 6, most models of cardiac tissue approximate the spatial domain as a continuum even though observation of cardiac tissue shows clearly that it is fundamentally discrete, composed of cells of different sizes and shapes that couple together. Although several approaches for representing cells discretely have been developed (Roberts et al., 2008; Spach et al., 2004; Stinstra et al., 2006), it is not yet known when such treatment is necessary. It will be important in the future to identify at what spatial resolution and under what conditions the continuum approximation is no longer valid for both monodomain and bidomain models, in tissues with anisotropy and, in 3-D, orthotropic fibre-sheet structure. A further consideration is the diverse cellular composition of cardiac tissue. Most current models of tissue electrophysiology represent only myocytes and neglect other cell types such as fibroblasts.

A challenge common to modelling communities is the level of methodological detail required for a scientific publication that describes a model of cardiac tissue electrophysiology. How much detail is necessary to describe a model of cardiac tissue electrophysiology, so that the results cannot only be conceived by a reader, but also reproduced for validation? Recently the MIRIAM (Le Novere et al., 2005) and MIASE (http://www.ebi.ac.uk/compneur-srv/miase/index.html) standards have been proposed, which specify the type of information that should be included when describing computational experiments at the cellular and sub-cellular level. Specific guidelines for models at the cardiac cell level have been proposed, which emphasise careful documentation of the underlying biophysics, relation of the model parameters to experimental data, numerical methods, and consistency of units in the model (Smith et al., 2007).

Although many of the simulation studies cited in this review report details and provenance of models and parameters, this attention to detail is not always the case. With rapid increases in available computing power and increasingly detailed simulation codes, it is possible to overlook the assumptions and parameter values that underlie a particular tissue scale model. On the basis of the issues raised in this review, we would propose that the following tentative list of should be included in descriptions of tissue electrophysiology models:

- Description of the model for cardiac cellular electrophysiology, referenced to the original cell model publication or model implementation such as the CellML model version curated at http://www.cellml.org, and with any changes to parameters justified and highlighted.
- Description of the tissue electrophysiology model, referenced to the original model publication and with a list of parameters that includes conductivities (or diffusion coefficients) and corresponding CV justified and linked to experimental measurements where possible.
- Numerical methods used to obtain solutions to the equations for cell and tissue electrophysiology, with evidence of numerical stability such as consistent CV with changes in time and space step.
- Links to source code, libraries, and other resources used in implementation of the model.
- Details of tissue geometry, including the source of anatomically detailed models, details of the meshing procedure and any image processing operations carried out on raw imaging data, information on spatial resolution, and, for FEM approaches, element size and shape.
- Evidence that tissue dynamics have been validated against either experimental data or comparable modelling data. For instance APD and CV restitution curves can be compared with other published data to demonstrate convergence.

This list is not intended to be proscriptive; rather our aim is to propose criteria to ensure that models of cardiac tissue electrophysiology are described in a consistent way:

8.2. Open questions

Different models of tissue electrophysiology involve different assumptions and simplifications, yet there is no generally accepted framework for choosing an appropriate combination of cellular electrophysiology model, tissue model, geometrical model, and numerical method. As discussed in Section 7.7, there is evidence that the choice of cellular electrophysiology model can influence tissue-level behaviours such as the stability of re-entry, however each of the areas listed below remain as open questions.

- **Choice of tissue model**. As discussed above (Section 4.2.3) both monodomain and bidomain tissue models can produce almost identical propagation sequences providing that no

current is injected into the extracellular space (Potse et al., 2006). However, there remain unresolved issues such as the role that boundary conditions play in the behaviour of re-entrant waves (Sambelashvilli and Efimov, 2004).

- **Numerical approach**. We have discussed the different numerical approaches that have been used to solve the equations of tissue electrophysiology, yet there are few studies where the influence of the numerical approach has been studied in a systematic way. A particular issue here is the possible influence of irregular and hybrid meshes on complex emergent behaviours such as re-entrant waves.
- **Benchmarks for numerical methods and implementations**. Related to the two questions described above is the lack of suitable benchmarks by which different tissue models and numerical approaches could be compared. A set of example problems, with accepted solutions, would be one solution.
- **Parameters and parameter sensitivity**. There are not well accepted values for parameters, such as the tissue conductivities, which are important in determining the behaviour of a propagating action potential. More work is needed not only to establish the biophysical basis for these parameters, but also to understand how sensitive the emergent phenomena discussed in section 5 are to variability in these parameters.
- **Methods for representing detailed and heterogeneous tissue micro-structure**. Cardiac tissue is a complex composite tissue, that is full of heterogeneity, yet it appears to behave as a functional syncytium. The roles played by fibroblasts, voids, and the fibre-sheet architecture of cardiac tissue in propagation of normal and abnormal activation remain unexplored in detail. Furthermore, appropriate parameters and boundary conditions for representing this complex structure are not well accepted, and it is likely that new numerical methods will need to be developed to handle abrupt changes in the orientation of fibres and sheets.
- **Representation of pathological structure and function**. This review has concentrated on models of normal tissue, although models of cardiac tissue electrophysiology have been widely used to study arrhythmias, which are usually associated with pathology. Robust methods and parameters to represent conditions including ischaemia, infarction, and heart failure are an important area that is not yet fully developed.
- **Validation against experimental data**. While it can be possible to validate simulated conduction velocity, activation sequence and restitution against published experimental data, many of the phenomena investigated using tissue models, such as the criteria for stable or unstable re-entry, are difficult to verify experimentally. As we have suggested above, a useful starting point for this process is to carefully compare model behaviour to experimental data where they exist, and to include this link in publications where models of tissue electrophysiology are used.

8.3. Conclusion

Models of cardiac tissue electrophysiology have played an important role in advancing our understanding of action potential propagation in the heart. Despite significant progress in the evaluation of modelling approaches, the efficient numerical treatment of models, and development of novel approaches, there are important challenges to be overcome for application and validation of these approaches in fields outside of their established domain.

Acknowledgements

This paper was conceived and drafted during a workshop on the Cardiac Physiome Project held at the Newton Institute for Mathematical Sciences at the University of Cambridge in July 2009 and funded by the Newton Institute, the UK Biotechnology and Biological Sciences Research Council, and the Wellcome Trust. FBS acknowledges support from the Nora Eccles Treadwell Foundation. AVP acknowledges support from the IHES and the James Simons Foundation. We thank Daniel Olmos Liceaga from the Departamento de Matemáticas, Universidad de Sonora, México for helpful comments on the manuscript. EMC and FHF acknowledge support from the National Science Foundation through grants no. 0824399 (EMC) and 0800793 (FHF and EMC) and through TeraGrid resources provided by the Pittsburgh Supercomputing Center.

References

Abildskov, J.A., 1976. Effects of activation sequence on the local recovery of ventricular excitability in the dog. Circulation Research 38, 240–243.
Abrahams, C., Janicki, J.S., Weber, K.T., 1987. Myocardial hypertrophy in Macaca fascicularis. Structural remodeling of the collagen matrix. Laboratory Investigation 56, 676–683.
Adler, C.P., Ringlage, W.P., Bohm, N., 1981. [DNA content and cell number in heart and liver of children. Comparable biochemical, cytophotometric and histological investigations (author's transl)]. Pathology, Research and Practice 172, 25–41.
Akar, F.G., Roth, B.J., Rosenbaum, D.S., 2001. Optical measurement of cell-to-cell coupling in intact heart using subthreshold electrical stimulation. American Journal of Physiology, Heart Circulatory Physiology 281, H533–H542.
Allexandre, D., Otani, N.F., 2002. Accuracy and speed considerations of a new numerical method for modeling cardiac excitation. Computers in Cardiology 29, 9–12.
Anderson, R.H., Ho, S.Y., 1998. The architecture of the sinus node, the atrioventricular conduction axis, and the internodal atrial myocardium. Journal of Cardiovascular Electrophysiology 9, 1233–1248.
Austin, T.M., Trew, M.L., Pullan, A.J., 2006. Solving the cardiac bidomain equations for discontinuous conductivities. IEEE Transactions on Biomedical Engineering 53, 1265–1272.
Banerjee, I., Yekkala, K., Borg, T.K., Baudino, T.A., 2006. Dynamic interactions between myocytes, fibroblasts, and extracellular matrix. Annals of New York Academy Sciences 1080, 76–84.
Banerjee, I., Fuseler, J.W., Price, R.L., Borg, T.K., Baudino, T.A., 2007. Determination of cell types and numbers during cardiac development in the neonatal and adult rat and mouse. American Journal of Physiology, Heart Circulatory Physiology 293, H1883–H1891.
Barr, R.C., Plonsey, R., 1984. Propagation of excitation in an idealized anisotropic two-dimensional tissue. Biophysical Journal 45, 1191–1202.
Beeler, G.W., Reuter, H., 1977. Reconstruction of the action potential of ventricular myocardial fibres. Journal of Physiology 268, 177–210.
Belhamadia, Y., Fortin, A., Bourgault, Y., 2009. Towards accurate numerical method for monodomain models using a realistic heart geometry. Mathematical Biosciences 220, 89–101.
Bernus, O., Wilders, R., Zemlin, C.W., Verschelde, H., Panfilov, A.V., 2002. A computationally efficient electrophysiological model of human ventricular cells. Americal Journal of Physiology (Heart and Circulatory Physiology) 282, H2296–H2308.
Bernus, O., Wellner, M., Pertsov, A.M., 2004. Intramural wave propagation in cardiac tissue: asymptotic solutions and cusp waves. Physical Review E 70, 061913.
Bers, D.M., 2008. Excitation-Contraction Coupling and Cardiac Contractile Force. Springer, Dordrecht.
Bondarenko, V.E., Szigeti, G.P., Bett, G.C.L., Kim, S., Rasmusson, R.L., 2004. Computer model of action potential of mouse ventricular myocytes. American Journal of Physiology (Heart and Circulatory Physiology) 287, H1378–H1403.
Bordas, R., Carpenteri, B., Fotia, G., Maggio, F., Nobes, R., Pitt-Francis, J., Southern, J., 2009. Simulation of cardiac electrophysiology on next-generation high-performance computers. Philosophical Transactions of the Royal Society A 367, 1951–1969.
Bourgault, Y., Ethier, M., LeBlanc, V.G., 2003. Simulation of electrophysiological waves with an unstructured finite element method. M2AN 37, 649–661.
Boyett, M.R., Tellez, J.O., Dobrzynski, H., 2009. The sinoatrial node:Its complex structure and unique ion channel gene program. In: Zipes, D.P., Jalife, J. (Eds.), Cardiac Electrophysiology: From Cell to Bedside, fifth ed. Saunders, Philadelphia, pp. 127–138.
Brette, F., Orchard, C., 2003. T-tubule function in mammalian cardiac myocytes. Circualtion Research 92, 1182–1192.
Bub, G., Shrier, A., Glass, L., 2002. Spiral wave generation in heterogenous excitable media. Physical Review Letters 88, 058101-1–058101-4.
Bueno-Orovio, A., Perez-Garcia, V.M., Fenton, F.H., 2006. Spectral methods for partial differential equations in irregular domains: the spectral smoothed boundary method. SIAM Journal on Scientific Computing 28, 886–900.
Bueno-Orovio, A., Cherry, E.M., Fenton, F.H., 2008. Minimal model for human ventricular action potentials in tissue. Journal of Theoretical Biology 253, 544–560.
Burton, R.A.B., Plank, G., Schneider, J.E., Grau, V., Ahammer, H., Keeling, S.J., Lee, J., Smith, N.P., Gavaghan, D., Trayanova, N., Kohl, P., 2006. 3-Dimensional models of individual cardiac histo-anatomy: tools and challenges. Annals of the New York Academy of Sciences 1380, 301–319.

Cabo, C., Pertsov, A.M., Baxter, W.T., Davidenko, J.M., Gray, R.A., Jalife, J., 1994. Wavefront curvature as a cause of slow conduction and block in isolated cardiac muscle. Circulation Research 75, 1014–1028.

Cabrera, J.A., Sanchez-Quintana, D., Ho, S.Y., Medina, A., Anderson, R.H., 1998. The architecture of the atrial musculature between the orifice of the inferior caval vein and the tricuspid valve: the anatomy of the isthmus. Jouranl of Cardiovascular Electrophysiology 9, 1186–1195.

Caldwell, B.J., Trew, M.L., Sands, G.B., Hooks, D.A., LeGrice, I.J., Smaill, B.H., 2009. Three distinct directions of intramural activation reveal nonuniform side-to-side electrical coupling of ventricular myocytes. Circulation Arrhythmia and Electrophysiology 2, 433–440.

Camelliti, P., Borg, T.K., Kohl, P., 2005. Structural and functional characterisation of cardiac fibroblasts. Cardiovascuar Research 65, 40–51.

Campbell, S.E., Gerdes, A.M., Smith, T.D., 1987. Comparison of regional differences in cardiac myocyte dimensions in rats, hamsters, and guinea pigs. Anatomical Record 219, 53–59.

Chen, L.S., Chen, P.-S., 2009. Nerve sprouting and cardiac arrhythmias. In: Zipes, D.P., Jalife, J. (Eds.), Cardiac Electrophysiology: From Cell to Bedside, fifth ed. Saunders, Philadelphia, pp. 381–390.

Cherry, E.M., Evans, S.J., 2008. Properties of two human atrial cell models in tissue: restitution, memory, propagation, and reentry. Journal of Theoretical Biology 254, 674–690.

Cherry, E., Fenton, F., 2004. Suppression of alternans and conduction blocks despite steep APD restitution: electrotonic, memory, and conduction velocity restitution effects. American Journal of Physiology (Heart and Circulatory Physiology) 286, 2332–2341.

Cherry, E.M., Fenton, F.H., 2007. A tale of two dogs: analyzing two models of canine ventricular electrophysiology. American Journal of Physiology (Heart and Circulatory Physiology) 292, H43–H55.

Cherry, E.M., Fenton, F.H., 2008. Visualization of spiral and scroll waves in simulated and experimental cardiac tissue. New Journal of Physics 10, 125016.

Cherry, E.M., Greenside, H.S., Henriquez, C.S., 2000. A space-time adaptive method for simulating complex cardiac dynamics. Physical Review Letters 84, 1343–1346.

Cherry, E.M., Greenside, H.S., Henriquez, C.S., 2003. Efficient simulation of three-dimensional anisotropic cardiac tissue using an adaptive mesh refinement method. Chaos 13, 853–865.

Cherry, E.M., Hastings, H.M., Evans, S.J., 2008. Dynamics of human atrial cell models: restitution, memory, and intracellular calcium dynamics in single cells. Progress in Biophysics & Molecular Biology 98, 24–37.

Chialvo, D.R., Michaels, D.C., Jalife, J., 1990. Supernormal excitability as a mechanism of chaotic dynamics of activation in cardiac Purkinje fibers. Cardiovascular Research 66, 525–545.

Chinchapatnam, P., Rhode, K., Ginks, M., Nair, P., Razavi, R., Arridge, S., Sermesant, M., 2009. Voxel based adaptive meshless method for cardiac eletrophysiology simulation. LNCS Functional Imaging and Modeling of the Heart 5528.

Clayton, R.H., Panfilov, A.V., 2008. A guide to modelling cardiac electrical activity in anatomically detailed ventricles. Progress in Biophysics & Molecular Biology 96, 19–43.

Colli Franzone, P., Pavarino, L., 2004. A parallel solver for reaction-diffusion systems in computational electrocardiology. Mathematical Models and Methods in Applied Sciences 14, 883–911.

Colli Franzone, P., Guerri, L., Pennacchio, M., Taccardi, B., 1998. Spread of excitation in 3-D models of the anisotropic cardiac tissue. II. Effects of fiber architecture and ventricular geometry. Mathematical Biosciences 147, 131–171.

Colli Franzone, P., Deuflhard, P., Erdmann, B., Lang, J., Pavarino, L.F., 2006. Adaptivity in space and time for reaction-diffusion systems in electrocardiology. SIAM Journal on Scientific Computing 28, 942–962.

Colli Franzone, P., Pavarino, L., Taccardi, B., 2005. Simulating patterns of excitation, repolarization and action potential duration with cardiac Bidomain and Monodomain models. Mathematical Biosciences 197, 35–66.

Conrath, C.E., Wilders, R., Coronel, R., De Bakker, J.M.T., Taggart, P., De Groot, J.R., Opthof, T., 2004. Intercellular coupling through gap junctions masks M cells in the human heart. Cardiovascular Research 62, 407–414.

Cooper, P.J., McKeever, S., Garny, A., 2006. On the application of partial evaluation to the optimisation of cardiac eletrophysiological simulations. In: In ACM Symposium on Partial Evaluation and Semantics Based Program Manipulation. ACM, Charleston South Carolina, pp. 12–20.

Courdiere, Y., Pierre, C., 2006. Stability and convergence of a finite volume method for two systems of reaction-diffusion equations in electro-cardiology. Nonlinear Analysis: Real World Applications 7, 916–935.

Courtemanche, M., Ramirez, R.J., Nattel, S., 1998. Ionic mechanisms underlying human atrial action potential properties: insights from a mathematical model. American Journal of Physiology (Heart and Circulatory Physiology) 275, H301–H321.

Courtemanche, M., 1996. Complex spiral wave dynamics in a spatially distributed ionic model of cardiac electrical activity. Chaos 6, 579–600.

Curtis, H.J., Cole, K.S., 1938. Transverse electrical impedance of the squid giant axon. Journal of General Physiology 21, 757–765.

Davies, P.F., 2009. Hemodynamic shear stress and the endothelium in cardiovascular pathophysiology. Nature Clinical Practice Cardiovascular Medicine 6, 16–26.

Delmar, M., Sorgen, P., 2009. Molecular organization and regulation of the cardiac gap junction channel connexin 43. In: Zipes, D.P., Jalife, J. (Eds.), Cardiac Electrophysiology: From Cell to Bedside, fifth ed. Saunders, Philadelphia, pp. 85–92.

Demmel, J., 1997. Applied Numerical Algebra. SIAM, Philadelphia.

Deuflhard, P., Erdmann, B., Roitzsch, R., Lines, G.T., 2009. Adaptive finite element simulation of ventricular fibrillation dynamics. Computing and Visualization in Science 12, 201–205.

Dierckx, H., Benson, A.P., Gilbert, S.H., Ries, M.E., Holden, A.V., Verschelde, H., Bernus, O., 2009. Intravoxel fibre structure of the left ventricular free wall and posterior left-right ventricular insertion site in canine myocardium using Q-ball imaging. Lecture Notes in Computer Science 5528, 495–504.

Dobrzynski, H., Li, J., Tellez, J., Greener, I.D., Nikolski, V.P., Wright, S.E., Parson, S.H., Jones, S.A., Lancaster, M.K., Yamamoto, M., Honjo, H., Takagishi, Y., Kodama, I., Efimov, I.R., Billeter, R., Boyett, M.R., 2005. Computer three-dimensional reconstruction of the sinoatrial node. Circulation 111, 846–854.

Durrer, D., van Dam, R.T., Freud, G.E., Janse, M.J., Meijler, F.L., Arzbaecher, R.C., 1970. Total excitation of the isolated human heart. Circulation 41, 899–912.

Efimov, I.R., Nikolski, V.P., Salama, G., 2004. Optical imaging of the heart. Circulation Research 286, H2183–H2194.

Endresen, K., Amlie, J.P., 1989. Electrical restitution and conduction intervals of ventricular premature beats in man: influence of heart rate. PACE 12, 1347–1354.

Endresen, K., Amlie, J.P., Forfang, K., Simonsen, S., Jensen, O., 1987. Monophasic action potentials in patients with coronary artery disease: reproducibility and electrical restitution and conduction at different stimulation rates. Cardiovascular Research 21, 696–702.

Ethier, M., Bourgault, Y., 2008. Semi-implicit time-discretization schemes for the bidomain model. SIAM Journal on Numerical Analysis 46, 2443–2468.

Faber, G.M., Rudy, Y., 2000. Action potential and contractility changes in Na+ (i) overloaded cardiac myocytes: a simulation study. Biophysical Journal 78, 2392–2404.

Fast, V.G., Kleber, A.G., 1993. Macroscopic conduction in cultured strands of neonatal rat heart cells measured with voltage-sensitive dyes. Circulation Research 73, 914–925.

Fawcett, D.W., McNutt, N.S., 1969. The ultrastructure of the cat myocardium. I. Ventricular papillary muscle. Journal of Cell Biology 42, 1–45.

Fenton, F., Karma, A., 1998. Vortex dynamics in three-dimensional continuous myocardium with fibre rotation: filament instability and fibrillation. Chaos 8, 20–47.

Fenton, F.H., Cherry, E.M., Hastings, H.M., Evans, S.J., 2002. Multiple mechanisms of spiral wave breakup in a model of cardiac electrical activity. Chaos 12, 852–892.

Fenton, F., Cherry, E., Karma, A., Rappel, W.-J., 2005. Modeling wave propagation in realistic heart geometries using the phase-field method. Chaos 15, 013502.

Fischer, G., Tilg, B., Modre, R., Huiskamp, G.J., Fetzer, J., Rucker, W., Wach, P., 2000. A bidomain model based BEM-FEM coupling formulation for anisotropic cardiac tissue. Annals of Biomedical Engineering 28, 1229–1243.

Fitzhugh, R., 1961. Impulses and physiological states in theoretical models of nerve membrane. Biophysical Journal 1, 445–466.

Fox, J.J., McHarg, J.L., Gilmour, R.F., 2002. Ionic mechanism of electrical alternans. American Journal of Physiology (Heart and Circulatory Physiology) 282, H516–H530.

Fozzard, H.A., Schoenberg, M., 1972. Strength–duration curves in cardiac Purkinje fibres: effects of liminal length and charge distribution. Journal of Physiology 226, 593–618.

Fozzard, H.A., 1966. Membrane capacity of the cardiac Purkinje fibre. Journal of Physiology 182, 255–267.

Gerardo-Giorda, L., Mirabella, L., Nobile, F., Perego, M., Veneziani, A., 2009. A model-based block-triangular preconditioner for the bidomain system in electrocardiology. Journal of Computational Physics 228, 3625–3639.

Gerdes, A.M., Moore, J.A., Hines, J.M., Kirkland, P.A., Bishop, S.P., 1986. Regional differences in myocyte size in normal rat heart. Anatomical Record 215, 420–426.

Gerhardt, M., Schuster, H., Tyson, J.J., 1990. A cellular automaton model of excitable media including curvature and dispersion. Science 247, 1563–1566.

Gerneke, D.A., Sands, G.B., Ganesalingam, R., Joshi, P., Caldwell, B.J., Smaill, B.H., Legrice, I.J., 2007. Surface imaging microscopy using an ultramiller for large volume 3D reconstruction of wax- and resin-embedded tissues. Microscopy Research and Technique 70, 886–894.

Gilbert, S.H., Benson, A.P., Li, P., Holden, A.V., 2007. Regional localisation of left ventricular sheet structure: integration with current models of cardiac fibre, sheet and band structure. European Journal of Cardiothoracic Surgery 32, 231–249.

Gilbert, S.H., Bernus, O., Holden, A.V., Benson, A.P., 2009. A quantitative comparison of the myocardial fibre orientation in the rabbit as determined by histology and by diffusion Tensor-MRI. Lecture Notes in Computer Science 5528, 49–57.

Girouard, S.D., Pastore, J.M., Laurita, K.R., Gregory, K.W., Rosenbaum, D.S., 1996. Optical mapping in a new guinea pig model of ventricular tachycardia reveals mechanisms for multiple wavelengths in a single reentrant circuit. Circulation 93, 603–613.

Goldsmith, E.C., Hoffman, A., Morales, M.O., Potts, J.D., Price, R.L., McFadden, A., Rice, M., Borg, T.K., 2004. Organization of fibroblasts in the heart. Developmental Dynamics 230, 787–794.

Gray, R.A., Pertsov, A.M., Jalife, J., 1998. Spatial and temporal organization during cardiac fibrillation. Nature 392, 75–78.

Greenberg, J.M., Hastings, S.P., 1978. Spatial patterns for discrete models of diffusion in excitablemedia. SIAM Journal on Applied Mathematics 34, 515–523.

Gumbiner, B.M., 1996. Cell adhesion: the molecular basis of tissue architecture and morphogenesis. Cell 84, 345–357.

Hackbusch, W., 1985. Multi-grid Methods and Applications. Springer, New York.
Hall Barbosa, C.R., 2003. Simulation of a plane wavefront propagating in cardiac tissue using a cellular automata model. Physics in Medicine and Biology 48, 4151–4164.
Hanson, B., Sutton, P., Elameri, N., Gray, M., Critchley, H., Gill, J.S., Taggart, P., 2009. Interaction of activation-repolarization coupling and restitution properties in humans. Circulation Arrhythmia and Electrophysiology 2, 162–170.
Harrild, D.M., Henriquez, C.S., 1997. A finite volume model of cardiac propagation. Annals of Biomedical Engineering 28, 315–334.
Helm, P., Faisal, M., Miller, M.I., Winslow, R.L., 2005. Measuring and mapping cardiac fiber and laminar architecture using diffusion tensor imaging. Annals of the New York Academy of Sciences 1047, 296.
Henriquez, C.S., Papazogou, A.A., 1996. Using computer models to understand the roles of tissue structure and membrane dynamics in arrhythmogenesis. Proceedings of the IEEE 84, 334–354.
Henriquez, C.S., Plonsey, R., 1990. Simulation of propagation along a cylindrical bundle of cardiac tissue. II. Results of simulation. IEEE Transactions on Biomedical Engineering 37, 861–875.
Henriquez, C.S., 1993. Simulating the electrical behavior of cardiac tissue using the bidomain model. Critical Reviews in Biomedical Engineering 21, 1–77.
Henry, H., Rappel, W.-J., 2004. The role of M cells and the long QT syndrome in cardiac arrhythmias: simulation studies of reentrant excitations using a detailed electrophysiological model. Chaos 14, 172–182.
Hinch, R., 2004. A mathematical analysis of the generation and termination of calcium sparks. Biophysical Journal 86, 1293–1307.
Hodgkin, A.L., Huxley, A.F., 1952. A quantitative description of membrane current and its application to conduction and excitation in nerve. Journal of Physiology (London) 117, 500–544.
Holden, A.V., Zhang, H., 1993. Modelling propagation and re-entry in anisotropic and smooth heterogeneous cardiac tissue. Journal of the Chemical Society Faraday Transactions 89, 2833–2837.
Holmes, A.A., Scollan, D.F., Winslow, R.L., 2000. Direct histological validation of diffusion tensor MRI in formaldehyde-fixed myocardium. Magnetic Resonance in Medicine 44, 157–161.
Hooke, N., Henriquez, C.S., Lanzkron, P., Rose, D., 1994. Linear algebraic transformations of the bidomain equations: implications for numerical methods. Mathematical Biosciences 120, 127–145.
Hort, W., 1957a. [Micrometric examination of guinea pig hearts of different width.]. Verh Dtsch Ges Kreislaufforsch 23, 343–346.
Hort, W., 1957b. [Research on muscle fiber dilation and the structure of the right heart chamber wall in a guinea pig.]. Virchows Archiv 329, 694–731.
Hort, W., 1960. [Macroscopic and micrometric research on the myocardium of the left ventricle filled to varying degrees.]. Virchows Archives of Pathology Anatomy and Physiology and Clinical Medicine 333, 523–564.
Hoyt, R.H., Cohen, M.L., Saffitz, J.E., 1989. Distribution and three-dimensional structure of intercellular junctions in canine myocardium. Circulation Research 64, 563–574.
Hsu, E.W., Muzikant, A.L., Matulevicius, S.A., Penland, R.C., Henriquez, C.S., 1998. Magnetic resonance myocardial fiber-orientation mapping with direct histological correlation. American Journal of Physiology (Heart and Circulatory Physiology) 274, 1627–1634.
Hucker, W.J., Ripplinger, C.M., Fleming, C.P., Fedorov, V.V., Rollins, A.M., Efimov, I.R., 2008. Bimodal biophotonic imaging of the structure-function relationship in cardiac tissue. Journal of Biomedical Optics 13, 054012.
Hucker, W.J., Dobrzynski, H., Efimov, I.R., 2009. Mechanisms of atrioventricular Nodal excitability and propagation. In: Zipes, D.P., Jalife, J. (Eds.), Cardiac Electrophysiology: From Cell to Bedside, fifth ed. Saunders, Philadelphia, pp. 249–258.
Hund, T.J., Rudy, Y., 2004. Rate dependence and regulation of action potential and calcium transient in a canine cardiac ventricular cell model. Circulation 110, 4008–4074.
Iyer, V., Mazhari, R., Winslow, R.L., 2004. A computational model of the human left-ventricular epicardial myocyte. Biophysical Journal 87, 1507–1525.
Jacquemet, V., Henriquez, C.S., 2005. Finite volume stiffness matrix for solving anisotropic cardiac propagation in 2-D and 3-D unstructured meshes. IEEE Transactions on Biomedical Engineering 52, 1490–1492.
Jie, X., Gurev, V., Trayanova, N., 2010. Mechanisms of mechanically induced spontaneous arrhythmias in acute regional ischaemia. Circulation Research 106, 185–192.
Jongsma, H.J., Wilders, R., 2000. Gap junctions in cardiovascular disease. Circulation Research 86, 1193–1197.
Ju, H., Dixon, I.M., 1996. Extracellular matrix and cardiovascular diseases. Canadian Journal of Cardiology 12, 1259–1267.
Keener, J.P., Bogar, K., 1998. A numerical method for the solution of the bidomain equations in cardiac tissue. Chaos 8, 234–241.
Keener, J.P., Sneyd, J., 1998. Mathematical Physiology. Springer-Verlag, New York.
Kleber, A.G., Rudy, Y., 2004. Basic mechanisms of cardiac impulse propagation and associated arrhythmias. Physiological Reviews 84, 431–488.
Kohl, P., Kamkin, A.G., Kiseleva, I.S., Noble, D., 1994. Mechanosensitive fibroblasts in the sino-atrial node region of rat heart: interaction with cardiomyocytes and possible role. Experimental Physiology 79, 943–956.
Kohl, P., Camelliti, P., Burton, F.L., Smith, G.L., 2005. Electrical coupling of fibroblasts and myocytes: relevance for cardiac propagation. Journal of Electrocardiology 38, 45–50.
Lampe, P.D., Fishman, G.I., 2009. Gap junction distribution and regulation in the heart. In: Zipes, D.P., Jalife, J. (Eds.), Cardiac Electrophysiology: From Cell to Bedside, fifth ed. Saunders, Philadelphia, pp. 307–316.
Lasher, R.A., Hitchcock, R.W., Sachse, F.B., 2009. Towards modeling of cardiac microstructure with catheter-based confocal microscopy: a novel approach for dye delivery and tissue characterization. IEEE Transactions on Medical Imaging 28, 1156–1164.
Le Novere, N., Finney, A., Hucka, M., Bhalla, U.S., Campagne, F., Collado-Vides, J., Crampin, E.J., Halstead, M., Klipp, E., Mendes, P., Nielsen, P.M., Sauro, H., Shapiro, B., Snoep, J.L., Spence, H.D., Wanner, B.L., 2005. Minimum information requested in the annotation of biochemical models (MIRIAM). Nature Biotechnology 23, 1509–1515.
LeGrice, I.J., Smaill, B.H., Chai, L.Z., Edgar, S.G., Gavin, J.B., Hunter, P.J., 1995. Laminar structure of the heart: ventricular myocyte arrangement and connective tissue architecture in the dog. American Journal of Physiology (Heart and Circulatory Physiology) 269, 571–582.
Li, J., Greener, I.D., Inada, S., Nikolski, V.P., Yamamoto, M., Hancox, J.C., Zhang, H., Billeter, R., Efimov, I.R., Dobrzynski, H., Boyett, M.R., 2008. Computer three-dimensional reconstruction of the atrioventricular node. Circulation Research 102, 975–985.
Lindemans, F.W., Zimmerman, A.E., 1979. Acute voltage, charge, and energy thresholds as functions of electrode size for electrical stimulation of the canine heart. Cardiovascular Research 13, 383–391.
Lodish, H., Berk, A., Matsudaira, P., Kaiser, C.A., Krieger, M., Scott, M.P., Zipursky, S.L., Darnell, J., 2003. Molecular Cell Biology. W.H. Freeman and Company, New York.
Lunkenheimer, P.P., Redmann, K., Kling, N., Jiang, X., Rothaus, K., Cryer, C.W., Wubbeling, F., Niederer, P., Heitz, P.U., Ho, S.Y., Anderson, R.H., 2006. Three-dimensional architecture of the left ventricular myocardium. The Anatomical Record. Part A, Discoveries in Molecular, Cellular, and Evolutionary Biology 288, 565–578.
Luo, C.-H., Rudy, Y., 1991. A model of the ventricular cardiac action potential. Depolarization, repolarization and their interaction. Circulation 68, 1501–1526.
Maclachlan, M.C., Sundnes, J., Spiteri, R.J., 2007. A comparison of non-standard solvers for ODEs describing cellular reactions in the heart. Computer Methods in Biomechanics and Biomedical Engineering 10, 317–326.
Mahajan, A., Shiferaw, Y., Sato, D., Baher, A., Olcese, R., Xie, L., Yang, M., Chen, P., Restrepo, J.G., Karma, A., Garfinkel, A., Qu, Z., Weiss, J.N., 2008. A rabbit ventricular action potential model replicating cardiac dynamics at rapid heart rates. Biophysical Journal 94, 392–410.
Mironov, S., Jalife, J., Tolkacheva, E.G., 2008. Role of conduction velocity restitution and short-term memory in the development of action potential duration alternans in isolated rabbit hearts. Circulation 118, 17–25.
Moe, G.K., Rheinboldt, W.C., Abildskov, J.A., 1964. A computer model of atrial fibrillation. American Heart Journal 67, 200–220.
Munteanu, M., Pavarino, L.F., Scacchi, S., 2009. A scalable Newton-Krylov-Schwarz method for the bidomain reaction–diffusion system. SIAM Journal on Scientific Computing 31, 3861–3883.
Murillo, M., Cai, X.-C., 2004. A fully implicit parallel algorithm for simulating the non-linear electrical activity of the heart. Numerical Linear Algebra with Applications 11, 261–277.
Nash, M.P., Bradley, C.P., Sutton, P.M., Clayton, R.H., Kallis, P., Hayward, M.P., Paterson, D.J., Taggart, P., 2006. Whole heart action potential duration restitution properties in cardiac patients: a combined clinical and modelling study. Experimental Physiology 91, 339–354.
Neal, M.L., Kerckhoffs, R., 2010. Current progress in patient-specific modeling. Breifings in Bioinformatics 11, 111–126.
Nerbonne, J.M., Guo, W., 2002. Heterogeneous expression of voltage-gated potassium channels in the heart: roles in normal excitation and arrhythmias. Journal of Cardiovascular Electrophysiology 13, 406–409.
Neu, J.C., Krassowska, W., 1993. Homogenization of syncytial tissues. Critical Reviews in Biomedical Engineering 21, 137–199.
Nickerson, D.P., Nash, M.P., Nielsen, P.M., Smith, N.P., Hunter, P.J., 2006. Computational multiscale modeling in the physiome project: modeling cardiac electromechanics. IBM Journal of Research and Development 50, 617–630.
Niederer, S.A., Smith, N.P., 2007. An improved numerical method for strong coupling of excitation and contraction models in the heart. Progress in Biophysics & Molecular Biology 96, 90–111.
Nielsen, P.M.F., LeGrice, I.J.E., Smaill, B.H., Hunter, P.J., 1991. Mathematical model of geometry and fibrous structure of the heart. American Journal of Physiology (Heart and Circulatory Physiology) 260, H1365–H1378.
Noble, D., Varghese, A., Kohl, P., Noble, P., 1998. Improved guinea pig ventricular cell model incorporating a dyadic space, IKr and IKs, and length and tension dependent processes. Canadian Journal of Cardiology 14, 123–134.
Noble, D., 1972. The relation of Rushton's 'liminal length' for excitation to the resting and active conductances of excitable cells. Journal of Physiology 226, 573–591.
Noble, D., 1979. The Initiation of the Heartbeat. Oxford University Press, Oxford.
Nygren, A., Fiset, C., Firek, L., Clark, J.W., Lindblad, D.S., Clark, R.B., Giles, W.R., 1998. Mathematical model of an adult human atrial cell: the role of K+ currents in repolarization. Circulation Research 82, 63–81.
Olivetti, G., Melissari, M., Capasso, J.M., Anversa, P., 1991. Cardiomyopathy of the aging human heart: myocyte loss and reactive cellular hypertrophy. Circulation Research 68, 1560–1568.
Olivetti, G., Cigola, E., Maestri, R., Corradi, D., Lagrasta, C., Gambert, S.R., Anversa, P., 1996. Aging, cardiac hypertrophy and ischemic cardiomyopathy do not affect the proportion of mononucleated and multinucleated myocytes in the human heart. Journal of Molecular and Cellular Cardiology 28, 1463–1477.

Osaka, T., Kodama, I., Tsuboi, N., Toyama, J., Yamada, K., 1987. Effects of activation sequence and anisotropic cellular geometry on the repolarization phase of action potential in the dog ventricles. Circulation 76, 226–236.
Owens, J.D., Luebke, D., Govindaraju, N., Harris, M., Kruger, J., Lefohn, A.E., Purcell, T.J., 2007. A survey of general-purpose computation on graphics hardware. Computer Graphics Forum 26, 80–113.
Pandit, S.V., Clark, R.B., Giles, W.R., Demir, S.S., 2001. A mathematical model of action potential heterogeneity in adult rat left ventricular myocytes. Biophysical Journal 81, 3029–3051.
Panfilov, A.V., Keener, J.P., 1995. Re-entry in three-dimensional Fitzhugh-Nagumo medium with rotational anisotropy. Physica D 84, 545–552.
Panfilov, A.V., Keldermann, R.H., Nash, M.P., 2007. Drift and breakup of spiral waves in reaction-diffusion-mechanics systems. Proceedings of the National Academy of Sciences of the United States of America 104, 7922–7926.
Panfilov, A.V., 2002. Sprial breakup in an array of coupled cells: the role of the intercellular conductance. Physical Review Letters 88, 118101.
Pavarino, L.F., Scacchi, S., 2008. Multilevel additive Schwarz preconditioners for the bidomain reaction–diffusion system. SIAM Journal on Scientific Computing 31, 420–443.
Penland, R.C., Harrild, D.M., Henriquez, C.S., 2002. Modeling impulse propagation and extracellular potential distributions in anisotropic cardiac tissue using a finite volume element discretization. Computing and Visualization in Science 4, 215–226.
Pennacchio, M., Simoncini, V., 2009. Algebraic multigrid preconditioners for the bidomain reaction-diffusion system. Applied Numerical Mathematics 59, 3033–3050.
Pennacchio, M., 2004. The mortar finite element method for the cardiac "bidomain" model of extracellular potential. Journal of Scientific Computing 20, 191–210.
Peskin, C.S., 1989. Fiber architecture of the left ventricular wall: an asymptotic analysis. Communications in Pure and Applied Mathematics 42, 79–113.
Plank, G., Liebmann, M., Weber dos Santos, R., Vigmond, E., Haase, G., 2007. Algebraic multigrid preconditioner for the cardiac bidomain model. IEEE Transactions on Biomedical Engineering 54, 585–596.
Plank, G., Zhou, L., Greenstein, J.L., Cortassa, S., Winslow, R.L., O'Rourke, B., Trayanova, N., 2008. From mitochondrial ion channels to arrhythmias in the heart: computational techniques to bridge the spatio-temporal scales. Philosophical Transactions of the Royal Society A 366, 3381–3409.
Plank, G., Burton, R.A.B., Hales, P., Bishop, M.J., Mansoori, T., Bernabeu, M.O., Garny, A., Prassl, A.J., Bollensdorff, C., Mason, F., Mahmood, F., Rodriguez, B., Grau, V., Schneider, J.E., Gavaghan, D., Kohl, P., 2009. Generation of histo-anatomically representative models of the individual heart: tools and application. Philosophical Transactions of the Royal Society A 367, 2257–2292.
Plonsey, R., Barr, R.C., 2000. Bioelectricity. A Quantitative Approach. Kluwer Academic, New York.
Poelzing, S., Akar, F.G., Baron, E., Rosenbaum, D.S., 2004. Heterogeneous connexin43 expression produces electrophysiological heteroegeneities across the ventricular wall. American Journal of Physiology (Heart and Circulatory Physiology) 296, H2001–H2009.
Poelzing, S., Roth, B.J., Rosenbaum, D.S., 2005. Optical measurements reveal nature of intercellular coupling across ventricular wall. American Journal of Physiology (Heart and Circulatory Physiology) 289, H1428–H1435.
Pollard, A.E., Barr, R.C., 1991. Computer simulations of activation in an anatomically based model of the human ventricular conduction system. IEEE Transactions on Biomedical Engineering 38, 982–996.
Pop, M., Sermesant, M., Lepiller, D., Truong, M.V., McVeigh, E.R., Crystal, E., Dick, A., Delingette, H., Ayache, N., Wright, G.A., 2009. Fusion of optical imaging and MRI for the evaluation and adjustment of macroscopic models of cardiac electrophysiology: a feasibility study. Medical Image Analysis 13, 370–380.
Pope, A.J., Sands, G.B., Smaill, B.H., LeGrice, I.J., 2008. Three-dimensional transmural organization of perimysial collagen in the heart. American Journal of Physiology (Heart and Circulatory Physiology) 295, H1243–H1252.
Potse, M., Dube, B., Richer, J., Vinet, A., Gulrajani, R.M., 2006. A comparison of monodomain and bidomain reaction-diffusion models for action potential propagation in the human heart. IEEE Transactions on Biomedical Engineering 53, 2425–2435.
Prassl, A.J., Kickinger, F., Ahammer, H., Grau, V., Schneider, J.E., Hofer, E., Vigmond, E., Trayanova, N.A., 2009. Automatically generated, anatomically accurate meshes for cardiac electrophysiology problems. IEEE Transactions on Biomedical Engineering 53, 2425–2435.
Press, W.H., Flannery, B.P., Teukolsky, S.A., Vetterling, W.T., 1992. Numerical Recipes in C. The Art of Scientific Computing. Cambridge University Press, Cambridge.
Priebe, L., Beuckelmann, D.J., 1998. Simulation study of cellular electrical properties in heart failure. Circulation Research 82, 1206–1223.
Pullan, A., Cheng, L.K., Buist, M.L., 2005. Mathematically Modelling the Eletrical Activity of the Heart: From Cell to Body Surface and Back Again. World Scientific, New Jersey.
Qu, Z.L., Garfinkel, A., 1999. An advanced algorithm for solving partial differential equation in cardiac conduction. IEEE Transactions on Biomedical Engineering 46, 1166–1168.
Quan, W., Evans, S.J., Hastings, H.M., 1998. Efficient integration of a realistic two-dimensional cardiac tissue model by domain decomposition. IEEE Transactions on Biomedical Engineering 45, 372–385.
Roberts, S.F., Stinstra, J.G., Henriquez, C.S., 2008. Effect of nonuniform interstitial space properties on impulse propagation: a discrete multidomain model. Biophysical Journal 95, 3724–3737.
Robinson, T.F., Cohen-Gould, L., Factor, S.M., 1983. Skeletal framework of mammalian heart muscle. Arrangement of inter- and pericellular connective tissue structures. Laboratory Investigation 49, 482–498.
Rodriguez, B., Li, L., Eason, J.C., Efimov, I.R., Trayanova, N., 2005. Differences between left and right ventricular chamber geometry affect cardiac vulnerability to electric shocks. Circulation Research 97, 168–175.
Rook, M.B., van Ginneken, A.C., de Jonge, B., el Aoumari, A., Gros, D., Jongsma, H.J., 1992. Differences in gap junction channels between cardiac myocytes, fibroblasts, and heterologous pairs. American Journal Physiology 263, C959–C977.
Roth, B.J., Wikswo, J.P., 1994. Electrical stimulation of cardiac tissue: a bidomain model with active membrane properties. IEEE Transactions on Biomedical Engineering 41, 232–240.
Roth, B.J., 1991. Action potential propagation in a thick strand of cardiac muscle. Circulation Research 68, 162–173.
Roth, B.J., 1997. Electrical conductivity values used with the bidomain model of cardiac tissue. IEEE Transactions on Biomedical Engineering 44, 326–328.
Roth, B.J., 2001. Meandering of spiral waves in anisotropic cardiac tissue. Physica D 150, 127–136.
Rudy, Y., 1995. Reentry – insights from theoretical simulations in a fixed Pathway. Journal of Cardiovascular Electrophysiology 6, 294–312.
Rush, S., Larsen, H., 1978. A practical algorithm for solving dynamic membrane equations. IEEE Transactions on Biomedical Engineering 25, 389–392.
Rushton, W.A.H., 1937. Initiation of the propagated disturbance. Proceedings of the Royal Society of London B 124, 210–243.
Saad, Y., 2003. Iterative Methods for Sparse Linear Systems, second ed. Society for Industrial and Applied Mathematics, Philadelphia.
Sachse, F.B., Moreno, A.P., Seemann, G., Abildskov, J.A., 2009. A model of electrical conduction in cardiac tissue including fibroblasts. Annals of Biomedical Engineering 37, 874–889.
Sambelashvilli, A., Efimov, I.R., 2004. Dynamics of virtual electrode-induced scroll-wave reentry in a 3D bidomain model. American Journal of Physiology (Heart and Circulatory Physiology) 287, H1570–H1581.
Sampson, K.J., Henriquez, C.S., 2005. Electrotonic influences on action potential duration dispersion in small hearts: a simulation study. American Journal of Physiology (Heart and Circulatory Physiology) 289, H350–H360.
Sands, G.B., Gerneke, D.A., Hooks, D.A., Green, C.R., Smaill, B.H., Legrice, I.J., 2005. Automated imaging of extended tissue volumes using confocal microscopy. Microscopy Research and Technique 67, 227–239.
Sato, D., Xie, Y., Weiss, J.N., Qu, Z., Garfinkel, A., Sanderson, A.R., 2009. Acceleration of cardiac tissue simulations with graphic processing units. Medical and Biological Engineering and Computing 47, 1011–1015.
Satoh, H., Delbridge, L.M., Blatter, L.A., Bers, D.M., 1996. Surface:volume relationship in cardiac myocytes studied with confocal microscopy and membrane capacitance measurements: species-dependence and developmental effects. Biophysical Journal 70, 1494–1504.
Savio-Galimberti, E., Frank, J., Inoue, M., Goldhaber, J.I., Cannell, M.B., Bridge, J.H., Sachse, F.B., 2008. Novel features of the rabbit transverse tubular system revealed by quantitative analysis of three-dimensional reconstructions from confocal images. Biophysical Journal 95, 2053–2062.
Schoenberg, M., Dominguez, G., Fozzard, H.A., 1975. Effect of diameter on membrane capacity and conductance of sheep cardiac Purkinje fibres. Journal of General Physiology 65, 441–458.
Scollan, D.F., Holmes, A., Zhang, J., Winslow, R.L., 2000. Reconstruction of cardiac ventricular geometry and fibre orientation using magnetic resonance imaging. Annals of Biomedical Engineering 28, 934–944.
Seemann, G., Hoper, C., Sachse, F.B., Dössel, O., Holden, A.V., Zhang, H., 2006. Heterogeneous three-dimensional anatomical and electrophysiological model of human atria. Philosophical Transactions of the Royal Society A 364, 1465–1481.
Seemann, G., Sachse, F.B., Karl, K., Weiss, D.L., Heuveline, V. and Dössel, O. Framework for modular, flexible and efficient solving the cardiac bidomain equation using PETSc. Progress in Industrial Mathematics at ECMI 2008, in press.
Shannon, T.R., Wang, F., Puglisi, J.L., Weber, C., Bers, D.M., 2004. A mathematical treatment of integrated Ca dynamics within the ventricular myocyte. Biophysical Journal 87, 3351–3371.
Shaw, R.M., Rudy, Y., 1995. The vulnerable window for unidirectional block in cardiac tissue: characterisation and dependence on membrane excitability and intercellular coupling. Journal of Cardiovascular Electrophysiology 6, 115–131.
Shaw, R.M., Rudy, Y., 1997a. Electrophysiologic effects of acute myocardial ischemia – a mechanistic investigation of action potential conduction and conduction failure. Circulation Research 80, 124–138.
Shaw, R.M., Rudy, Y., 1997b. Ionic mechanisms of propagation in cardiac tissue – roles of the sodium and L-type calcium currents during reduced excitability and decreased gap junction coupling. Circulation Research 81, 727–741.
Smith, J.M., Cohen, R.J., 1984. Simple finite-element model accounts for a wide range of cardiac dysrhythmias. Proceedings of the National Acadamy of Sciences 81, 233–237.
Smith, N.P., Crampin, E.J., Niederer, S.A., Bassingthwaighte, J.B., Beard, D.A., 2007. Computational biology of cardiac myocytes: proposed standards for the physiome. Journal of Experimental Biology 210, 1576.
Smith, R.M., Matiukas, A., Zemlin, C.W., Pertsov, A.M., 2008. Nondestructive optical determination of fiber organization in intact myocardial wall. Microsc Res Tech 71, 510–516.
Spach, M.S., Heidlage, J.F., Darken, E.R., Hofer, E., Raines, K.H., Starmer, C.F., 1992. Cellular Vmax reflects both membrane properties and the load presented by adjoining cells. American Journal of Physiology (Heart and Circulatory Physiology) 263, H1855–H1863.

Spach, M.S., Heidlage, J.F., Dolber, P.C., Barr, R.C., 2000. Electrophysiological effects of remodeling cardiac gap junctions and cell size: experimental and model studies of normal cardiac growth. Circulation Research 86, 302–311.

Spach, M.S., Heidlage, J.F., Barr, R.C., Dolber, P.C., 2004. Cell size and communication: role in structural and electrical development and remodeling of the heart. Heart Rhythm 1, 500–515.

Stevens, C., Hunter, P., 2003. Sarcomere length changes in a 3D mathematical model of the pig ventricles. Progress in Biophysics and Molecular Biology 82, 229–241.

Stinstra, J.G., Hopenfeld, B., MacLeod, R.S., 2005. On the passive cardiac conductivity. Annals of Biomedical Engineering V33, 1743–1751.

Stinstra, J.G., Roberts, S.F., Pormann, J.B., Macleod, R.S., Henriquez, C.S., 2006. A model of 3D propagation in discrete cardiac tissue. Computers in Cardiology 33, 41–44.

Strang, G., 1968. On the construction and comparison of difference schemes. SIAM Journal on Numerical Analysis 5, 506–517.

Streeter, D.D.J., Spotnitz, H.M., Patel, D.P., Ross, J.J., Sonnenblick, E.H., 1969. Fiber orientation in the canine left ventricle during diastole and systole. Circulation Research 24, 339–347.

Sundnes, J., Lines, G.T., Mardal, K.A., Tveito, A., 2002. Multigrid block preconditioning for a coupled system of partial differential equations modeling the electrical activity in the heart. Computer Methods in Biomechanics and Biomedical Engineering 5, 397–409.

Sundnes, J., Lines, G.T., Tveito, A., 2005. An operator splitting method for solving the bidomain equations coupled to a volume conductor model for the torso. Mathematical Biosciences 194, 233–248.

Sundnes, J., Artebrant, R., Skavhaug, O., Tveito, A., 2009. A second-order algortihm for solving dynamic cell membrane equations. IEEE Transactions on Biomedical Engineering 56.

Szentadrassy, N., Banyasz, T., Biro, T., Szabo, G., Toth, B.I., Magyar, J., Lazar, J., Varro, A., Kovacs, L., Nanasi, P.P., 2005. Apico–basal inhomogeneity in distribution of ion channels in canine and human ventricular myocardium. Cardiovascular Research 65, 851–860.

Ten Tusscher, K.H.W.J., Bernus, O., Hren, R., Panfilov, A.V., 2006. Comparison of electrophysiological models for human ventricular cells and tissues. Progress in Biophysics & Molecular Biology 90, 326–345.

Ten Tusscher, K.H.W.J., Mourad, A., Nash, M.P., Clayton, R.H., Bradley, C.P., Paterson, D.J., Hayward, M.P., Panfilov, A.V., Taggart, P., 2009. Organization of ventricular fibrillation in the human heart: experiments and models. Experimental Physiology 94, 553–562.

TenTusscher, K.H.W.J., Noble, D., Noble, P.J., Panfilov, A.V., 2004. A model for human ventricular tissue. American Journal of Physiology (Heart and Circulatory Physiology) 286, H1573–H1589.

Trangenstein, J.A., Kim, C., 2004. Operator splitting and adaptive mesh refinement for the Luo-Rudy I model. Journal of Computational Physics 196, 645–679.

Trayanova, N., 2006. Defibrillation of the heart: insights into mechanisms from modelling studies. Experimental Physiology 91, 323–337.

Trew, M., Grice, I.L., Smaill, B., Pullan, A., 2005a. A finite volume method for modeling discontinuous electrical activation in cardiac tissue. Annals of Biomedical Engineering V33, 590–602.

Trew, M.L., Smaill, B.H., Bullivant, D.P., Hunter, P.J., Pullan, A.J., 2005b. A generalized finite difference method for modeling cardiac electrical activation on arbitrary, irregular computational meshes. Mathematical Biosciences 198, 169–189.

van Kempen, M.J., Fromaget, C., Gros, D., Moorman, A.F., Lamers, W.H., 1991. Spatial distribution of connexin43, the major cardiac gap junction protein, in the developing and adult rat heart. Circulation Research 68, 1638–1651.

Vetter, F.J., McCulloch, A.D., 1998. Three dimensional analysis of regional cardiac function: a model of rabbit ventricular anatomy. Progress in Biophysics & Molecular Biology 69, 157–183.

Victorri, B., Vinet, A., Roberge, F.A., Drouhard, J.P., 1985. Numerical integration in the reconstruction of cardiac action potentials using Hodgkin-Huxley-type models. Computers and Biomedical Research 18, 10–23.

Vigmond, E.J., Leon, L.J., 1999. Computationally efficient model for simulating electrical activity in cardiac tissue with fiber rotation. Annals of Biomedical Engineering 27, 160–170.

Vigmond, E., Aguel, F., Trayanova, N., 2002. Computational techniques for solving the bidomain equations in three dimensions. IEEE Transactions on Biomedical Engineering 49, 1260–1269.

Vigmond, E., Weber dos Santos, R., Prassl, A.J., Deo, M., Plank, G., 2008. Solvers for the cardiac bidomain equations. Progress in Biophysics & Molecular Biology 96, 3–18.

Vigmond, E.J., Boyle, P.M., Leon, L., Plank, G., 2009. Near-real-time simulations of bioelectric activity in small mammalian hearts using graphical processing units. Conference Proceedings: IEEE Engineering in Medicine and Biology Society 1, 3290–3293.

Viswanathan, P.C., Shaw, R.M., Rudy, Y., 1999. Effects of I-Kr and I-Ks heterogeneity on action potential duration and its rate dependence – a simulation study. Circulation 99, 2466–2474.

Waller, I., Kapral, R., 1984. Spatial and temporal structure in systems of couple nonlinear oscillators. Physical Review A 30, 2047–2055.

Weber dos Santos, R., Plank, G., Bauer, S., Vigmond, E., 2004a. Parallel multigrid preconditioner for the cardiac bidomain model. IEEE Transactions on Biomedical Engineering 51, 1960–1968.

Weber dos Santos, R., Plank, G., Bauer, S., Vigmond, E., 2004b. Preconditioning techniques for the bidomain equations. Lecture Notes in Computational Science and Engineering 40, 571–580.

Weber, K.T., Sun, Y., Tyagi, S.C., Cleutjens, J.P., 1994. Collagen network of the myocardium: function, structural remodeling and regulatory mechanisms. Journal of Molecular and Cellular Cardiology 26, 279–292.

Whiteley, J.P., 2006. An efficient numerical technique for the solution of the monodomain and bidomain equations. IEEE Transactions on Biomedical Engineering 53, 2139–2147.

Whiteley, J.P., 2008. An efficient technique for the numerical solution of the bidomain equations. Annals of Biomedical Engineering 36, 1398–1408.

Wiener, N., Rosenblueth, A., 1946. The mathematical formations of the problem of conduction of impulse in a network of connected elements, specifically in cardiac muscle. Archivos del Instituto de Cardiologa de Mexico 16, 205–265.

Wikswo, J.P., Lin, S.F., Abbas, R.A., 1995. Virtual electrodes in cardiac tissue: a common mechanism for anodal and cathodal stimulation. Biophysical Journal 73, 2195–2210.

Winfree, A.T., 1998. A spatial scale factor for electrophysiological models of myocardium. Progress in Biophysics & Molecular Biology 69, 185–203.

Winslow, R.L., Varghese, A., Noble, D., Adlakha, C., Hoythya, A., 1993. Generation and propagation of ectopic beats induced by spatially localized Na–K pump inhibition in atrial network models. Proceedings of the Royal Society of London B 254, 55–61.

Winslow, R.L., Rice, J., Jafri, M.S., Marban, E., O'Rourke, B., 1999. Mechanisms of altered excitation-contraction coupling in canine tachycardia-induced heart failure, II: model studies. Circulation Research 84, 571–586.

Xu, A., Guevara, M.R., 1998. Two forms of spiral-wave re-entry in an ionic model of ischaemic myocardium. Chaos 8, 157–174.

Yue, A.M., Franz, M.R., Roberts, P.R., Morgan, J.M., 2005. Global endocardial electrical restitution in human right and left ventricles determined by noncontact mapping. Journal of the American College of Cardiology 46, 1067–1075.